Distinct oxygenation modes of the Gulf of Oman during the past 43,000 years – a multi-proxy approach

Nicole Burdanowitz[1], Gerhard Schmiedl[1], Birgit Gaye[1], Philipp M. Munz[2], Hartmut Schulz[2]

[1] Institute for Geology, Center for Earth System Research and Sustainability (CEN), Universität Hamburg, Bundesstraße 55, 20146 Hamburg, Germany
[2] Department of Geosciences, Eberhard Karls Universität Tübingen, Hölderlinstr. 12, 72074 Tübingen, Germany

Correspondence to: Nicole Burdanowitz (nicole.burdanowitz@uni-hamburg.de)

Abstract.

Changing Cclimatic conditions and its changecan shape the strength and extent of the oxygen minimum zone (OMZ). The presence and variability of the OMZ in the Arabian Sea is of importance for itstheir ecosystem. The state of oxygenation has, for instance, an impact on the pelagic and benthic faunal community or the nitrogen and carbon cycles. It is important to understand the dynamics of the OMZ and related marine environmental conditions because of The understanding of the dynamics of the OMZ, its marine environmental is of importance due to its climate feedbacks. In this study, we combined three independent proxies to reconstruct the oxygenation state of the water column and bottom water in the Gulf of Oman for the past about 43 ka. This multi-proxy approach is done for the first time at the northeast Oman margin located in the Gulf of Oman. We used bulk sedimentary nitrogen isotopes ($\delta^{15}N$) as well as the alkane ratio (lycopane + n-C$_{35}$)/n-C$_{31}$ and benthic foraminiferal faunal analysis to reconstruct the strength of the OMZ in the water column and bottom water oxygenation, respectively. Our results show that the Gulf of Oman experienced strong pronounced OMZ and bottom water deoxygenation during the Holocene. ContraryIn contrast, during the Last Glacial Maximum (LGM)/ Marine Isotope Stage (MIS) 2 the Gulf of Oman was very well ventilated with a highly diverse benthic foraminiferal community. This may have been caused by stronger wind-induced mixing and better ventilation by oxygen-rich water masses. Our results also show moderate oxygenation during MIS 3 with deoxygenation events during most of the warmer Dansgaard-Oeschger (D/O) events. We propose two distinct oxygenation modes for the Gulf of Oman: 1) a stable period of either strongly pronounced water column OMZ and bottom water deoxygenation or well-oxygenated water column and bottom water conditions and 2) an unstable period of oscillating oxygenation states between moderately oxygenated (stadials) and deoxygenated (interstadial, D/O events) conditions. The unstable period may be triggered by an interstadial AMOC mode, which is required to initiate D/O events.

1 Introduction

Oxygen minimum zones (OMZs) are an important feature of the oceans. Although they cover only about 8 % of the total oceanic surface (Paulmier and Ruiz-Pino, 2009), they have a great impact on the marine environment and the carbon and nitrogen cycles (Friederich et al., 2008; Gruber, 2004; Paulmier et al., 2011; Rixen et al., 2020; Wakeham, 2020). For instance,

denitrification plays a major role in the nitrogen cycle of OMZs and denitrification also acts isas the largest sink for nitrogen in the ocean (Gruber, 2004; Rixen et al., 2020). Moreover, OMZs have the potential to act as a source for greenhouse gases like N₂0N₂O, CO_2 or CH_4 (Friederich et al., 2008; Naqvi et al., 2010; Paulmier and Ruiz-Pino, 2009). Further, several studies show that the intensification and deoxygenation of OMZs are positively coupled to climate warming (e.g. Bopp et al., 2013; Breitburg et al., 2018; Busecke et al., 2022; Zhou et al., 2022). One of the strongest OMZ is located in the Arabian Sea comprising about 17 % of the worldwide area of OMZs (Rixen et al., 2020). Over half of the permanently hypoxic shelf sediments are located in the northern Indian Ocean affecting benthic ecosystems, for instance, the diversity of benthic foraminifera (Helly and Levin, 2004; Levin, 2003). Although the diversity of benthic foraminifera is generally reduced under low oxygen conditions, the OMZ faunas of the Arabian Sea seem to be more resilient to low oxygen conditions when compared to other non-OMZ regions. This higher resilience can be attributed to a dominance of nitrate respiring infaunal benthic foraminifera in OMZ regions (Schmiedl et al., 2023).

The Gulf of Oman, as part of the Arabian Sea, is a complex and poorly understood region. It is influenced by the intrusion of warm, highly saline and more oxygenated Persian Gulf Water (PGW), when compared to the Arabian Sea water. Different gyres in the Gulf of Oman and their seasonal variations lead to a patchy distribution of the PGW in this area (Pous et al., 2004; Wang et al., 2013). Little is known about the oceanic environmental conditions in the past and its response to climate change in this region as only a few sedimentary records and modelling studies exist (Cullen et al., 2000; Lachkar et al., 2019; Schmidt et al., 2020; Sirocko et al., 1991; Staubwasser et al., 2003). According to Lachkar et al. (2019), rising sea surface temperatures (SSTs) in the Persian Gulf, especially during the winter month, reduce the ability of the PGW to ventilate the upper OMZ in the Gulf of Oman due to shallower spreading of the PGW. The authors also concluded that a strengthening of the OMZ in the Gulf of Oman can be also induced by lower sea level. In this scenario, the Persian Gulf has fallen dry and, therefore, With a dry Persian Gulf, the OMZ in the Gulf of Oman would also strengthen as the ventilation via the PGW would stop completely (Lachkar et al., 2019). However, existing Holocene and late Pleistocene sedimentary records (cores M5/3a – 422 & Orgon4-KS8, Sirocko et al., 1991, 2000; Staubwasser et al., 2003) located below the OMZ in the Gulf of Oman do not investigate the oxygenation status in this area. Nevertheless, from sedimentary records in other parts of the Arabian Sea OMZ we know that the OMZ varied in its extend and volume during the past (Altabet et al., 2002; Böll et al., 2014; Burdanowitz et al., 2019; Gaye et al., 2018; Ivanochko et al., 2005; Möbius et al., 2011; Pichevin et al., 2007; Suthhof et al., 2001). Those records have shown a greater expansion of the OMZ during the Holocene (interstadial), also known as Marine Isotope Stage 1 (MIS 1), than during the Last Glacial Maximum (LGM, MIS 2) and stadials of MIS 3. Further, most of the rapid warming events of the Dansgaard-Oeschger (D/O) events during the last glacial period resulted in a strengthening of the OMZ, albeit each single D/O event had a different impact on local scale (Altabet et al., 2002; Ivanochko et al., 2005; Pichevin et al., 2007). However, due to the lack of continuous high-resolution archives in the Gulf of Oman, little is known about the OMZ and bottom water oxygenation prior to the Holocene, especially without the influence of Persian Gulf Water (PGW) in this area.

Most of the records are based on the qualitative reconstruction of the oxygenation status. The most common used proxy is the bulk $\delta^{15}N$ of marine sediments. The global average $\delta^{15}N$ of deep-water nitrate is about 4.8 ± 0.2 ‰ but in intermediate and

65   surface water the $\delta^{15}N$ of nitrate can deviate strongly from this value due to the isotopic fractionation associated with nitrogen cycling processes (Sigman et al., 2000; Sigman and Fripiat, 2019). In oxygen depleted environments heterotrophic bacteria use nitrate as an electron acceptor to oxidize organic matter and reduce the nitrogen in several steps to nitrogen gas (Sigman and Fripiat, 2019). Denitrification is associated with a strong isotopic effect of 15-25 ‰ so that the residual nitrate becomes strongly enriched in ^{15}N and can thus have $\delta^{15}N$ values >20 ‰ (Casciotti, 2016). Upward mixing and upwelling can transport

70   this enriched isotopic signal where it is incorporated into phytoplankton. ~~It is coupled to the denitrification in the water column with more elevated values due to less oxygen and, therefore, stronger denitrification and vice versa (Rixen et al., 2020 and references therein).~~ During the nitrate consumption, phytoplankton also uses the lighter ^{14}N with an isotope discrimination factor of about 5 ‰ and incorporate the denitrification signal into the biomass (Montoya, 2008). After decease of the biomass and sinking to the ocean floor, the denitrification signal is transported to the seafloor and can be stored in the sediments (e.g.

75   Altabet et al., 1995; Gaye-Haake et al., 2005). Therefore, $\delta^{15}N$ values can be used as a proxy for the OMZ strength in the water column (e.g. Altabet et al., 1995; Reichart et al., 1997). However, diagenetic processes can alter sedimentary $\delta^{15}N$ values especially under low sedimentation rates (Gaye-Haake et al., 2005; Jung et al., 1997; Junium et al., 2015; Möbius et al., 2011; Tesdal et al., 2013). Nevertheless, it was found that in the Arabian Sea, especially under high sedimentation rates on the shelf and slope, sedimentary $\delta^{15}N$ values are a reliable indicator for past denitrification processes (Möbius et al., 2011).

80   Another rarely used biomarker is the isoprenoid hydrocarbon lycopane, which is mainly limited to sediments from OMZs or oceanic anoxic events in the past (van Bentum et al., 2009; Dummann et al., 2021; Farrington et al., 1988; Ogihara, 2014; Sabino et al., 2020, 2021; Sinninghe Damsté et al., 2003). It is discussed that probably photoautotrophic organisms produce lycopane, but its origin is not yet fully resolved (Freeman et al., 1994; Sinninghe Damsté et al., 2003; Wakeham et al., 1993). However, these studies have shown that lycopane is well preserved in anoxic environments and is fast degraded under oxic

85   conditions. Lycopane often co-elutes with the *n*-alkane *n*-C_{35} (van Bentum et al., 2009; Naeher et al., 2012; Sabino et al., 2020; Sinninghe Damsté et al., 2003), with the latter mainly produced by terrestrial plants (e.g. Eglinton and Hamilton, 1967; Meyers and Ishiwatari, 1993). An unusual high abundance of *n*-C_{35} and lycopane (if co-eluted) or lycopane alone were detected in some parts of the Arabian Sea with highest contents within the OMZ (Schulte et al., 1999, 2000; Sinninghe Damsté et al., 2003). Therefore the (lycopane + *n*-C_{35})/*n*-C_{31} ratio can be used as indicator for bottom water oxygenation with ratios > 0.5

90   representing suboxic to anoxic conditions (van Bentum et al., 2009; Sinninghe Damsté et al., 2003). Whereas these two presented proxies are a qualitative way to reconstruct the OMZ strength and bottom water oxygenation, benthic foraminifera can be used to achieve a quantitative oxygenation status reconstruction. The different benthic foraminifera species with their broad specific oxygen level requirements are widely used to reconstruct past bottom water oxygen conditions (e.g. Fontanier et al., 2002; Jorissen et al., 1995; Koho et al., 2008; Kranner et al., 2022; Lu et al., 2023; Schmiedl et al., 2000, 2010).

95   Here, we present the first high-resolution record reconstructing the OMZ strength and oxygen status of the bottom water at a depth situated within the present OMZ for the Holocene and late Pleistocene (past approx. 43 ka) at the Oman margin in the Gulf of Oman by using a multi-proxy approach.

2 Modern oceanographic setting in the study area

The Gulf of Oman as part of the northwestern Arabian Sea connects the Arabian Sea via the Strait of Hormuz with the Persian Gulf. The northern Arabian Sea and the Gulf of Oman are affected by different water masses. At the surface, the Arabian Sea High-Salinity Water (ASHSW) with salinities between 35.3 and 36.7 comprises the upper 200 m (Kumar and Prasad, 1999; Shenoi et al., 1993). The highly saline (> 36.5) low-oxygen PGW is responsible for a weak ventilation of the upper OMZ (Figure 1, 150-300 m water depth), especially in the southern part of the Gulf of Oman (Bower et al., 2000; Kumar and Prasad, 1999; Morrison et al., 1998; Pous et al., 2004; Prasad et al., 2001; Schmidt et al., 2020; Shenoi et al., 1993; Wang et al., 2013). The Red Sea Water (RSW, salinity: 35.1 – 35.6) enters the Arabian Sea via the Gulf of Aden and is found at intermediate water depths between 600 to 900 m (Bower et al., 2000; Kumar and Prasad, 1999). The RSW is transported northward along the Oman coast, especially during the SW monsoon (Acharya and Panigrahi, 2016; Beal et al., 2000; Kumar and Prasad, 1999; Schmidt et al., 2020). Other Iintermediate water masses (500 – 1000 m water depth) consist ofare the Indian Central Water (ICW), which is a mixture of the Antarctic Intermediate Water (AAIW) and the Indonesian Intermediate Water (IIW), and enters the Arabian Sea during the SW monsoon via the Somali current along the Somali and Arabian coasts (Acharya and Panigrahi, 2016; Schott and McCreary, 2001). The initial oxygen-rich ICW becomes less oxygenated during its transport to the Arabian Sea (Acharya and Panigrahi, 2016). However, the oxygen content is still higher than those of the PGW and RSW (Rixen et al., 2014).

The region is influenced by different atmospheric circulations, which result in different seasonal primary productivity patterns (Figure 2). During the summer season, strong southwest (SW) winds and the Findlater Jet in the western Arabian Sea induce upwelling and lateral transport of cold nutrient-rich water resulting in high primary productivity (Figure 2b) (Andruleit et al., 2003; Haake et al., 1993; Rixen et al., 2020). In contrast, highest productivity in the northern Arabian Sea and Gulf of Oman is observed during the winter season (Figure 2d) when high amounts of nutrients are available due to deeper wind-induced surface mixing by the NE winds (Böll et al., 2014; Madhupratap et al., 1996; Rixen et al., 2020). During the summer season, the Ras Al Hadd Jet at the northeastern corner of Oman can transport cold upwelled water into the Gulf of Oman via eddies (Schott and McCreary, 2001). Further, eddies generated in the Gulf of Oman transport PGW trapped in its core into the Arabian Sea (L'Hégaret et al., 2015; de Marez et al., 2019). Both may have an impact on the sea surface temperature, salinity and primary productivity in this region.

3 Material and methods

The 739 cm long gravity core SL167 was collected in the northwestern Arabian Sea from the continental northeastern Oman margin off northern Oman (Gulf of Oman, 22°37.15'N, 59°41.49'E, 774 m water depth) during RV *Meteor* cruise M74/1b in 2007 (Figure 1). In total, 371 samples were used for $\delta^{15}N$ analyses with continuous sampling intervals of 2 cm. For lipid biomarker analyses 225 samples were used with an interval of 2 cm in the upper 162 cm of the core and, due to low total organic carbon content (unpublished), an interval of 4 cm below 162 cm. All sediment samples were freeze-dried and

130 homogenized with an agate mortar and pestle prior to chemical treatment for the analyses. For the analyses of benthic foraminifera, 149 samples taken every 5 cm were used.

3.1 Dating & age model

The age model is based on twenty-one radiocarbon datings by accelerator mass spectrometry (AMS) measurements of surface-dwelling planktonic foraminifera, comprising *Globigerinoides spp.*, *Globigerinella spp.* and *Orbulina universa,* at Beta

135 Analytic Inc, Miami, USA. The age-depth model was developed by using the Bayesian model package BACON v.2.5.6 (Blaauw and Christen, 2011) within R statistical software (v.4.3, R Core Team (2023)). We used the default settings except for accumulation mean (set to 50), memory mean (set to 0.3) and the calibration curve (set to Marine20). We applied a deltaR (ΔR) of 93 ± 61 years. The ΔR is based on the weighted mean of two regional marine reservoir corrections (Muscat) by Southon et al. (2002) using the marine calibration database (Reimer and Reimer, 2001, http://calib.org/marine/).

140 ### 3.2 Bulk nitrogen isotope ($\delta^{15}N$) analyses

For the $\delta^{15}N$ analyses 6 to 61 mg of the freeze-dried and homogenized sediment were weighted into Sn-capsules. $\delta^{15}N$ were obtained by combusting the samples at 1050°C in a Thermo Scientific Flash EA1112 elemental analyser coupled to a Finnigan MAT 252 isotope ratio mass spectrometer. Nitrogen was calibrated against the International Atomic Energy Agency (IAEA) reference standard IAEA-1 and IAEA-2, respectively. In addition to an internal standard, both (IAEA-1 and IAEA-2) were

145 used as working standards. Replicate measurements of these standards yielded a precision better than 0.2 ‰. The samples were measured in duplicate with a mean standard deviation of 0.07 ‰.

3.3 2 Lipid biomarker analyses

Total lipid extracts (TLE) of about 3 to 18 g of the sediment samples were obtained by using a DIONEX Accelerated Solvent Extractor (ASE 200) at 100°C and 1000 PSI for 5 minutes (3 cycles) using a solvent mixture of dichloromethane:methanol

150 (DCM:MeOH, 9:1) following the procedure described in (Herrmann et al., (2016). Prior to extraction a known amount of an internal standard (squalene) was added to the samples. After the extraction, TLEs were concentrated via rotary evaporation and transferred to combusted 4 ml vials. We have used $NaSO_4$ column chromatography to separate the TLEs into a hexane-insoluble and hexane-insoluble fraction. Therefore, a combusted Pasteur pipette was packed with cleaned cotton wool and about 2 cm $NaSO_4$. The column was then first cleaned with about 8 ml hexane. Then TLE was transferred with about 1 ml

155 hexane to the column and the remaining 4 ml vial was cleaned 3 times with about 1 ml hexane, which was also transferred to the column. For the hexane-insoluble fraction, about 1 ml of DCM was added for 4 times on the column. The latter hexane-soluble was saponified (85°C, 2 h) in a 5 % potassium hydroxide (KOH) in MeOH solution and the neutral fraction wasere extracted with hexane. To obtain the *n*-alkane containing apolar fraction from the neutral fraction, a column chromatography packed with deactivated silica gel (5 % H_2O, 60 mesh) was carried out by using hexane as solvent. Afterwards, the apolar

160 fraction was cleaned with hexane via column chromatography packed with silver nitrate coated silica gel ($AgNO_3$-Si).

For quantification of the *n*-alkanes a Thermo Scientific Trace 1310 gas chromatography coupled to a flame ionization detector (GC-FID) equipped with a Thermo Scientific TG-5MS column (30 m, 0.25 mm, 0.25 µm). The carrier gas H_2 with a flow rate of 35 ml min^{-1} was used. The PTV injector was operated starting at 50°C ramped with 10°C s^{-1} to 325°C in a splitless mode. The initial GC temperature was programmed to 50°C (held 3 min) and then to increase with 6°C min^{-1} to a final temperature of 325°C, which was held for 20 minutes. For quantification of *n*-alkanes an external standard containing the *n*-C_8 – *n*-C_{40} alkanes was used in a known concentration. Quantification precision of repeated analyses of the external standard was 8 %.

The mass spectra of two samples (14 – 16 cm and 182 – 186 cm) were investigated with a Thermo Scientific Trace GC Ultra coupled to a Thermo Scientific DSQ II mass spectrometer (GC-MS) with He (2 ml min^{-1} flow rate) as carrier gas. The initial GC temperature of 50°C was held for 3 minutes and ramped with 6°C min^{-1} to 325°C with the final temperature hold for 25 minutes. To identify the compounds of the apolar fraction the mass spectra were compared with published mass spectral data.

The average chain length (ACL) of plant-wax derived *n*-alkanes are commonly used to identify plant functional types and environmental conditions (e.g. Collister et al., 1994; Cooper et al., 2015; Eglinton and Eglinton, 2008; Rommerskirchen et al., 2006). For instance, plants located in arid environments tend to have longer ACL than plants in humid environments (e.g. Carr et al., 2014; Rommerskirchen et al., 2006; Vogts et al., 2009). But the ACL also differs with the plant functional type, for instance C4 grasses have in general higher ACL than woody gymnosperms (e.g. Bush and McInerney, 2013; Carr et al., 2014; Cooper et al., 2015). However, the validity of the ACL is limited and, if possible, should be combined with compound-specific isotope measurements of the *n*-alkanes (e.g. Eglinton and Eglinton, 2008; Rommerskirchen et al., 2006; Vogts et al., 2009). We have calculated the ~~average chain length~~ (ACL~~)~~ of *n*-alkanes using following equation:

$$ACL_{27-33} = \frac{27 \times C_{27} + 29 \times C_{29} + 31 \times C_{31} + 33 \times C_{33}}{C_{27} + C_{29} + C_{31} + C_{33}} \qquad (1)$$

The carbon preference index (CPI), an indicator for the odd-over-even predominance, is usable to distinguish between terrestrial plant and petroleum sources (e.g. Bray and Evans, 1961; Cranwell, 1978, 1981; Pancost and Boot, 2004). Terrestrial plant derived *n*-alkanes and recent sediments with unaltered organic material have an odd-over-even predominance with a CPI higher than 3 (e.g. Bray and Evans, 1961). In contrast, petroleum sources have higher abundance of even *n*-alkanes with CPIs < 1 and are an indication of higher degradation (e.g. Bray and Evans, 1961). The CPI ~~was~~ calculated by using the following equation:

$$CPI_{27-33} = 0.5 \times \left(\frac{C_{27} + C_{29} + C_{31} + C_{33}}{C_{26} + C_{28} + C_{30} + C_{32}} + \frac{C_{27} + C_{29} + C_{31} + C_{33}}{C_{28} + C_{30} + C_{32} + C_{34}} \right) \qquad (2)$$

where Cx is the concentration of the *n*-alkane with x atoms.

3.~~2~~3 Bulk nitrogen isotope ($\delta^{15}N$) analyses

For the $\delta^{15}N$ analyses, following the procedure described in ~~(~~Menzel et al., ~~(~~2014), 6 to 61 mg of the freeze-dried and homogenized sediment were weighted into Sn-capsules. $\delta^{15}N$ were obtained by combusting the samples at 1050°C in a Thermo Scientific Flash EA1112 elemental analyser coupled to a Finnigan MAT 252 isotope ratio mass spectrometer. Nitrogen was

calibrated against the International Atomic Energy Agency (IAEA) reference standard IAEA-1 and IAEA-2, respectively. In addition to an internal standard, both (IAEA-1 and IAEA-2) were used as working standards. Replicate measurements of these standards yielded a precision better than 0.2 ‰. The samples were measured in duplicate with a mean standard deviation of
195 0.07 ‰.

3.4 Benthic foraminifera analyses

For faunal analyses, between 198 and 558 (average of 311) individuals were at each depth counted from representative splits of the size fraction >125 µm. Species assignment is mainly based on Jones (1994), Den Dulk (2000), Szarek (2001), Schumacher et al. (2007) and Debenay (2012). Allochthonous shelf taxa, including larger benthic foraminifera (e.g., genera
200 *Amphistegina*, *Heterostegina, Borelis, Peneroplis*), typical neritic taxa (e.g., *Ammonia* spp., *Cibicides refulgens*, *Elphidium* spp., *Lobatula lobatula*), and taxa with floating chambers (genera *Cymbaloporetta*, *Millettiana*, *Tretomphalus*, *Tretomphaloides*) were removed from the census data set (Murray, 1991). For benthic foraminiferal diversity, the Shannon Index H(S) was calculated according to Buzas and Gibson (1969). The H(S) considers the number of species and their relative proportion in the sample. The H(S) value is at a maximum, when all species have equal proportions, while species with low
205 abundances contribute little to it. In eutrophic to mesotrophic ecosystems, the diversity and microhabitat structure is oxygen-controlled, as predicted by the TROX (Trophic-Oxygen) model (Gooday, 2003; Jorissen et al., 1995) (Figure 3). For the estimation of bottom-water oxygenation, the different taxa were classified into oxic, suboxic, and dysoxic taxa based on their modern microhabitat preferences (Table S1) (Schmiedl et al., 2023). Bottom-water oxygen concentrations were then calculated based on the Enhanced Benthic Foraminiferal Oxygen Index (EBFOI) and associated transfer function of Kranner et al. (2022)
210 with the modification of (Schmiedl et al., (2023). The mean standard deviation (SD) across the entire oxygen range (0-6 ml l^{-1}) is ±0.61 ml l^{-1}. However, SD is lower at suboxic to dysoxic conditions, with SD of ±0.49 and ±0.08 ml l^{-1} across oxygen ranges of 1-2 ml l^{-1} and 0-1 ml l^{-1}, respectively. The expected relation between oxygen concentration and benthic foraminiferal diversity is clearly expressed at core site SL167, since it is influenced by comparatively high organic matter fluxes and low oxygen conditions (Figure 3).

215 ### 3.5 Statistics

To identify periodicities in our data sets we performed spectral and wavelet analyses in R (v.4.3, R Core Team (2023)). For the spectral analysis, we used the REDFIT function of the package dplR v.1.7.4 (Bunn et al., 2022; Bunn, 2008, 2010) which is based on the Fortran 90 REDFIT source code by Schulz and Mudelsee (2002). For the wavelet analysis the data sets were first interpolated to an even spaced data set by using the package ncdf4.helpers v.0.3-6 (Bronough, 2021) and the approx.
220 function. The wavelet analysis were performed with the package biwavelet v.0.20.21 (Gouhier et al., 2021) using the morlet wavelet function and bias-corrected power spectrum which is based on Torrence and Compo (1998).

4 Results

4.1 Age model of SL167

The results of the AMS radiocarbon measurements are shown in Table 1. The core SL167 comprises the last about 42.6 ka (Figure 4Figure 3). However, the last 3 ka BP are missing in the core as the core top represents ca. 3.1 ka BP. The mean sedimentation rates range between 0.10 mm/year and 0.49 mm/year with higher sedimentation rates during the Holocene compared to the Pleistocene.

4.2 Lipid biomarker and $\delta^{15}N$ reconstructions

The samples of SL167 show a strong odd-over even carbon number predominance with CPI values ranging between 2 and 13.8 and show a dominance of land-plant derived long chain n-alkanes, where the ACL_{27-33} varies between 30 and 31.2 (Fig. A1). In some samples, for land-plant derived n-alkanes, unusual high contents of the n-alkane C_{35} were detected in the GC-FID chromatograms. We chose one exemplary sample with a very high content of n-C_{35} and one sample with a usual distribution of land plant derived n-alkanes for mass spectral analyses, respectively. For the latter one we found only the mass spectra of the n-alkane C_{35} at the expected retention time. However, for the sample with the high n-C_{35} content and unusual n-alkane distribution pattern, we found both, the mass spectra of lycopane (2,6,10,14,19,23,27,31-octamethyldotriacontane) and of n-C_{35} (Figure 5Figure 4). The characteristic fragments of lycopane are the ions m/z 113, 183, 253, 309, 337, 407 and 447 (Sinninghe Damsté et al., 2003), which are also detected in our sample with the co-elution of n-C_{35} and lycopane (Figure 5Figure 4b). It is known from other studies that n-C_{35} and lycopane can co-elute during gas chromatography measurements (van Bentum et al., 2009; Sabino et al., 2020; Sinninghe Damsté et al., 2003).

The (lycopane + n-C_{35})/n-C_{31} varies between 0.1 and 1.7 throughout the core (Figure 6d). Highest ratios occur during the late Holocene (3 – 4 ka BP) and warmer Pleistocene periods reconstructed by the NGRIP ice core $\delta^{18}O$ (North Greenland Ice Core Project members, 2004) and Sofular cave $\delta^{13}C$ (Fleitmann et al., 2009) records, respectively.

The $\delta^{15}N$ values in our Gulf of Oman record vary between 4.7 and 9.2 ‰ (Figure 6Figure 5b) with constant high values throughout the Holocene (> 7.2 ‰). The variability of $\delta^{15}N$ is high (4.5 ‰) during the Pleistocene with higher values > 7 ‰ during warmer phases. reconstructed by the NGRIP ice core $\delta^{18}O$ (North Greenland Ice Core Project members, 2004) and Sofular cave $\delta^{13}C$ (Fleitmann et al., 2009) records, respectively.

4.3 Benthic foraminiferal diversity and reconstructed bottom-water oxygenation

Overall, the benthic foraminiferal diversity is high and ranges between H(S)=1.94 and 4.27 (average of 3.31 ± 0.64 SD). Significant fluctuations occur in the older part of the core with minima during interstadials, while Heinrich events H2 and H1, and the Last Glacial Maximum are characterized by comparatively high H(S) values (Figure 6Figure 5). During the Holocene, the H(S) values exhibit a gradual decrease. The reconstructed oxygen values range between 0.27 and 3.25 (average of 1.46 ± 0.74 SD) and are negatively correlated to the benthic foraminiferal diversity and $\delta^{15}N$. D/O events, the B/A and Holocene are

characterized by relatively low oxygen concentrations while cold intervals, particularly the interval around H1, exhibit higher values (Figure 6Figure 5).

255

5 Discussion

The $\delta^{15}N$ is often used as indicator for past denitrification processes and, in the Arabian Sea, strength of the OMZ (e.g. Altabet et al., 2002; Gaye et al., 2018; Ivanochko et al., 2005; Möbius et al., 2011; Pichevin et al., 2007). However, the $\delta^{15}N$ signal can be biased by different processes, which need to be considered. One factor is a diagenetic overprint of $\delta^{15}N$ leading to an enrichment of the heavier ^{15}N isotope, especially under low sedimentation rates (3 – 4 cm kyr^{-1}) (Altabet et al., 1999; Gaye-Haake et al., 2005; Jung et al., 1997; Junium et al., 2015; Möbius et al., 2011; Tesdal et al., 2013). In contrast, shelf and slope sediments deposited under high sedimentation rates in the Arabian Sea are considered to have unaltered $\delta^{15}N$ values and, therefore, a reliable indicator for past denitrification processes (Möbius et al., 2011). The sedimentation rates are high in SL167and varies between 9.7 and 49 cm kyr^{-1}. Further, they correlate with the nitrogen content but not with $\delta^{15}N$ values (Fig. A2). The correlation of the nitrogen content and $\delta^{15}N$ may due to higher productivity and/or better preservation of organic matter under sub-/anoxic conditions. Therefore, we argue that sedimentary $\delta^{15}N$ in SL167 are a reliable indicator for past denitrification process. However, it may be possible that the $\delta^{15}N$ signal in SL 167 is affected by changes in the water mass transport, mixing or lateral transport from e.g. the Oman Upwelling area.

5.1 Strength of the OMZ and bottom water oxygenation in the Gulf of Oman

270
5.1.1 Pleistocene

Both independent proxies for bottom water oxygenation, (lycopane + n-C$_{35}$)/n-C$_{31}$ ratio, the O$_2$ reconstruction by benthic foraminifera, and the Shannon diversity index, are in very good agreement at least for the Pleistocene part of the core (Figure 6Figure 5a, c & d). Phases of sub-/anoxic bottom water match well with observed interstadials, the D/O events, in the Greenland ice core records, e.g. NGRIP (North Greenland Ice Core Project members, 2004), except for D/O 6 and 7. Most intenseHighest reconstructed bottom water oxygenation oxygen content (up to 3.2 ml l^{-1}) occurred from about 14.3 to 19.6 ka BP and during the Younger Dryas between 11.2 and 12.3 ka BP, respectively (Figure 6Figure 5c). Further, MIS 3 (about 25 ka – 43 ka BP), is characterized by several distinct peaks of a strong OMZ (Figure 6Figure 5b) in the water column. Note, that we used the Sofular $\delta^{13}C$ cave record from Turkey (Fleitmann et al., 2009) instead of the NGRIP to allocate the distinct D/O events as it seems to be more appropriate (Figure 7Figure 6). Fleitmann et al. (2009) found a systematic age offset for most D/O events between the NGRIP and the more regional Sofular and Hulu cave (China) records by several centennial years, with younger ages for the D/O events in the NGRIP record. The D/O events 3-5 and 8-11 are well pronounced as strong abrupt OMZ intervals in the Gulf of Oman. In contrast, in the nearby Oman upwelling (core RC27-14) all D/O events, except 11, are expressed as strong OMZ intervals in the water column (Figure 7Figure 6c) (Altabet et al., 2002). A high-resolution record

(MD04-2876) in the northern Arabian Sea shows a similar pattern as core RC27-14 (Pichevin et al., 2007), whereas a record
(NIOP905) from the more southern Somali Upwelling area (Ivanochko et al., 2005) does not show a strong OMZ in the water
column during the first four D/O events (Figure 7~~Figure 6~~b & d). Note that shifts in OMZ peaks of the different records in the
Arabian Sea may be due to age uncertainty as well as peak tuning of the other records with the Greenland ice core (GISP2)
δ^{18}O record.

Bottom water oxygenation may not only be driven by processes in the upper water column but also by the occurrence of
different water masses. The RSW is transported northward especially during the SW monsoon (Acharya and Panigrahi, 2016;
Beal et al., 2000; Kumar and Prasad, 1999) and may undergo oxygen depletion due to higher organic matter supply and its
decay on its way to the Gulf of Oman (Pathak et al., 2021). Acharya and Panigrahi (2016) have shown, that today's RSW core
extends between 600 and 660 m reaching nearly the seafloor at the core site (~740 m). Thus, phases with stronger SW
monsoons, such as the D/O interstadials, are characterized by more input of low oxygen RSW and, therefore, sub-/anoxic
conditions of bottom water in the Gulf of Oman. This corroborates findings from the Oman Upwelling area, where oxygen
bottom water reconstructions using benthic foraminifera show oxygen depleted conditions during phases with higher outflow
of RSW into the northwestern Arabian Sea (Pathak et al., 2021).

The missing D/O 6 and weak D/O 7 events might be a result of the combination of local/regional and global conditions. First,
the strength of the Indian and Asian Monsoon systems are strongly coupled to high latitude climate (e.g. Deplazes et al., 2013,
2014; Overpeck et al., 1996; Schulz et al., 1998; Singh et al., 2011; Wang et al., 2001). Phases with strong monsoon intervals
are coupled to the D/O events found in Greenland ice cores. However, duration and strength of both varied through the time.
In some records from the Asian region, D/O 6 had a weaker environmental impact than other D/O events (e.g. Deplazes et al.,
2014; Ivanochko et al., 2005; Wang et al., 2001). Second, the fluctuation of the Red Sea sea level (Figure 7~~Figure 6~~f) could
lead to variations in the exchange of the RSW and the Indian Ocean/Arabian Sea, with stronger influence during higher sea
level and vice versa (Arz et al., 2007; Siddall et al., 2003). However, the sea level was in general lower during MIS 3 than
during the Holocene, which might led to a weaker influence of the RSW compared to recent conditions (Rohling et al., 2008;
Siddall et al., 2003). Third, the degree of northward extension of the oxygen-rich AAIW is linked to North Atlantic climate
(Jung et al., 2009; Pahnke and Zahn, 2005). The maxima in the northward extension and, therefore, ventilation of the Arabian
Sea water column are found during the Heinrich stadials. In contrast, minima extension occurred during interstadials with a
stronger monsoon (Jung et al., 2009). In total, the interplay of this three mentioned factors, ~~and~~ the bipolar seesaw structure of
the northern and southern hemispheric climate but also the climate and oceanic patterns on regional scale~~signals~~ (e.g. Lemieux-
Dudon et al., 2010; Stocker and Johnsen, 2003), may lead to the feature that some of the D/O events as well as Heinrich events
(H4) are not represented in the Gulf of Oman record. Further, stronger northwesterly as well as northeasterly winds during
stadials (Leuschner and Sirocko, 2000) could have induced stronger deep winter mixing compared to present and, therefore,
better ventilation (Lu et al., 2023; Reichart et al., 1998).

A striking feature of our Gulf of Oman δ^{15}N record is the prominent triple peak of strong water column deoxygenation from
D/O events 3 to 5 (Figure 6b). This is in contrast to other Arabian Sea records, not showing a prominent triple peak from D/O

events 3 to 5 but 5 to 7 with a broader D/O 8 event beforehand (Schulz et al., 1998). Interestingly, at the core site sub-/anoxic bottom water conditions occurs during D/O 2, whereas the OMZ in the water column was not developed. We speculate that the inflow of oxygen depleted RSW into the Gulf of Oman was still strong and/or the maxima northward extension of the ventilating AAIW/ICW was further south, while denitrification processes were not as strong as during other pronounced D/O events. This is also the case for a record from the southern Somali Upwelling area (Figure 7Figure 6d). However, along the Oman Upwelling area (Altabet et al., 2002), a strong SW monsoon could have favoured upwelling-induced denitrification and therefore a strengthening of the OMZ only in this region, albeit not as strong as during former D/O events.

In contrast to other parts of the Arabian Sea, the water column in the Gulf of Oman was well ventilated during the whole LGM indicated by low $\delta^{15}N$ values (Figure 7Figure 6) and by high benthic foraminiferal diversity (Figure 6Figure 5). The northern and northeastern Arabian Sea experienced a stronger and/or longer NE monsoon season during the LGM (Pichevin et al., 2007; Suthhof et al., 2001). Thus, the stronger wind-induced mixing may have resulted in a better-ventilated OMZ compared to the interstadials. A recent study from the Oman Upwelling area also suggests slightly increased oxygenation in the upper water column (~600 – 820 m) during the LGM compared to the modern interstadial (Lu et al., 2023). Further, less lateral transport of nutrient- and oxygen-poor waters from the Oman Upwelling due to weakened SW winds was supposed to mitigate denitrification in the northern and northeastern Arabian Sea (Suthhof et al., 2001). In addition, a northward expansion of the well oxygenated AAIW during stadials results in a better-ventilated intermediate waters in the Arabian Sea, reducing the strength of the OMZ (Jung et al., 2009; Pichevin et al., 2007). However, the productivity was still high enough to maintain an OMZ. The absence of the OMZ at the core location from the LGM to the beginning of the Bølling/Allerød (B/A) may be due to more intense northwesterly winds in the Gulf of Oman and NE monsoon (Leuschner and Sirocko, 2000; Sirocko et al., 2000) leading to stronger wind-induced mixing and ventilation of the water column. Weak Indian summer monsoonISM phases occurred also during the LGM in NE India (Dutt et al., 2015) and the eastern Arabian Sea (Saravanan et al., 2020). In addition, Red Sea sea level was too low during that time (Sergiou et al., 2022; Siddall et al., 2003) to induce significant RSW influence on bottom water deoxygenation in the Gulf of Oman. The Persian Gulf plays no role in contributing water masses to the Gulf of Oman as it was nearly completely dry until the LGM and had no connection to the Gulf of Oman (Lambeck, 1996; Stoffers and Ross, 1979).

During the B/A interstadial, a strong OMZ and bottom water oxygenation occurred in the Gulf of Oman and was also observed for the whole Arabian Sea (Altabet et al., 2002; Ivanochko et al., 2005; Kessarkar et al., 2013; Orsi et al., 2017; Pichevin et al., 2007; Suthhof et al., 2001). Contrary to the O$_2$ reconstruction of the benthic foraminifera we see no distinct high ratios of (lycopane + n-C$_{35}$)/n-C$_{31}$ during the B/A. Here it is possible that the threshold of oxygen depletion was not reached to preserve lycopane in the sediment.

5.1.2 Holocene

In contrast, the highest ratios of (lycopane + n-C$_{35}$)/n-C$_{31}$ (> 1.0) occurred during the late Holocene, which may be due to relatively high total organic carbon mass accumulation rates during that time (Fig. A1) and thus is an effect of fast burial. This

is also corroborated by the increasing dominance of the opportunistic food indicator *Uvigerina peregrina* (Koho et al., 2008; Schmiedl et al., 2010) during the late Holocene, leading to decreasing benthic foraminiferal diversity.

The observed low reconstructed O_2 contents and high $\delta^{15}N$ values with minor fluctuations during the Holocene indicate a continuously strong OMZ and sub-/anoxic bottom water in at the Oman margin area in the Gulf of Oman. This is in line with other studies for most parts of the Arabian Sea (Figure 7Figure 6, Altabet et al., 2002; Burdanowitz et al., 2019; Gaye et al., 2018; Kessarkar et al., 2013; Pichevin et al., 2007; Suthhof et al., 2001). In the course of the post LGM sea level rise, the Persian Gulf became connected to the Gulf of Oman via the Strait of Hormuz at around 13 ka BP with flooding the central part of the Persian Gulf until about 11.5 ka BP (Lambeck, 1996). At least, since the Mid-Holocene, the PGW is an important factor in ventilating the upper OMZ (150 – 300 m) in the northern Arabian Sea (Lachkar et al., 2019). However, modern data show a relatively low increase of O_2 content (about 0.5 mol l^{-1}) due to PGW at (Figure 1) and near the core location (Munz et al., 2017).

Highest ratios of (lycopane + n-C_{35})/n-C_{31} (> 1.0) occurred during the late Holocene, which may be due to relatively high total organic carbon mass accumulation rates during that time (Fig. A1) and thus is an effect of fast burial. This assumption is also corroborated by the increasing dominance of the opportunistic food indicator *Uvigerina peregrina* (Koho et al., 2008; Schmiedl et al., 2010) which favours high supply of organic matter, leading to decreasing benthic foraminiferal diversity.

Overall, our multi-proxy oxygen record for the Gulf of Oman shows striking features. First, during most interstadial periods (D/O events and Holocene) the denitrification/OMZ in the water column as well as bottom water deoxygenation was strong. Second, during MIS 3 oxygen conditions oscillate between moderately oxygenated (glacial) and deoxygenated/denitrification conditions (interglacial, D/O events) marking this period as an environmentally unstable period. Here, the oxygen concentrations were close to the threshold of suboxic/anoxic conditions and therefore fluctuated between oxia and suboxia driven by changes in monsoon strength. In contrast, LGM/MIS 2 and the Holocene period show quite constant oxygen and deoxygenation/denitrification conditions, respectively. We argue that these two periods are stable enough to suppress strong oscillations of oxygenation versus deoxygenation.

5.2 Periodic changes and potential global drivers for OMZ strength and bottom water oxygenation

In order to identify specific periodicities, we have performed spectral- and wavelet analyses for the $\delta^{15}N$ record (Figure 8Figure 7) and the oxygen (O_2) reconstruction of the benthic foraminifera (Figure 9Figure 8), respectively. For the strength of the OMZ in the water column based on $\delta^{15}N$, we have found significant (95 % confidence interval (CI)) periods of 3.8 ka, 3.2 ka, 2.7 ka, 1.3 ka, 1.1 ka as well as 690 and 570 years (Figure 8Figure 7a). For the reconstructed O_2 bottom water variations, we have found significant periods (95 % CI) of 1.14 ka, 710, 670, 600 and 570 years as well as 3.17 2 ka (90 % CI, Figure 9Figure 8a). These periods are mainly present between about 25 ka – 43 ka BP (MIS 3) and 8 ka – 16 ka BP (Transition LGM/MIS 2 to Holocene, Figure 8Figure 7b & Figure 9Figure 8b) for both proxies. We attribute the periods of about 1.1 – 1.3 ka as well as around 3.2 ka to the D/O events as they occur with periods of about 1.5 ka and 3.0 ka (Kuniyoshi et al., 2022; Schulz, 2002).

Especially the period of around 1.5 ka is a widespread feature in climate records (e.g. Bond et al., 2001; Jaglan et al., 2021;
Lauterbach et al., 2014; Leuschner and Sirocko, 2000; Saravanan et al., 2020; Thamban et al., 2007; Wang et al., 2005).
However, Obrochta et al. (2012) question the general idea of a 1.5 ka oscillation as they propose a superposition of the 1.0 ka
and 2.0 ka cycles, which is also evident in our record with the 1.1 to 1.3 ka periods. Another strong evidence for D/O events
as trigger of these periods is that the D/O events are also absent during the LGM/MIS 2 period (Buizert and Schmittner, 2015;
North Greenland Ice Core Project members, 2004). The cold phase and its high global ice volume during the LGM inhibited
an interstadial AMOC mode (strong AMOC/warm North Atlantic), which is required to initiate D/O events (Buizert and
Schmittner, 2015). An interesting feature is the successive decrease in duration and magnitude of the D/O events between two
Heinrich events (Buizert and Schmittner, 2015). However, this pattern ~~might~~ may or may not be the reason for the missing
D/O 6 signal in our record as D/O 5 is strong and the last event between H4 and H3.

The periods of 570 to 710 years can be related to solar cycles (Liu et al., 2012; Stuiver and Braziunas, 1993; Wang et al.,
2005a). These cycles are prominent worldwide and also found in the East Asian (Liu et al., 2012; Wang et al., 1999, 2005a;
Xu et al., 2014) and Indian Monsoon (Burdanowitz et al., 2021; Neff et al., 2001; von Rad et al., 1999; Saravanan et al., 2020;
Sarkar et al., 2000; Thamban et al., 2007) realms, respectively. Some authors attribute a 725-775 years periodicity to changes
in the Indian summer monsoon ~~ISM~~ (Saravanan et al., 2020), ENSO-like cycles (Russell et al., 2003) or a harmonic cycle of
the 1500 year cycle (von Rad et al., 1999), linked to the thermohaline circulation (Wang et al., 1999) or to the ITCZ movement
in the tropics (Russell and Johnson, 2005). Most of the high frequency periods (< 1000 years) are reported for the Holocene
(Burdanowitz et al., 2021; Liu et al., 2012; Neff et al., 2001; von Rad et al., 1999; Russell et al., 2003; Russell and Johnson,
2005; Stuiver and Braziunas, 1993; Thamban et al., 2007; Wang et al., 1999, 2005b; Xu et al., 2014) or the LGM (Saravanan
et al., 2020). Here we show that these high frequency periods are also present during MIS 3. The intensity and position of the
monsoon system is driven by the summer insolation (precession signal) and the latitudinal ~~insolation~~ temperature gradient
(~~LTG,~~ obliquity signal), respectively, with the latter influenced by the latitudinal insolation gradient (~~LIG~~) and ice cover (Davis
and Brewer, 2009). The authors postulate that a strong latitudinal temperature gradient~~LTG~~ moves the monsoon system
towards the equator, which was the case during the LGM/MIS 2 for the summer (ca. 20 – 28 ka BP) and winter (ca. 18 – 25
ka BP) latitudinal temperature gradients~~LTG~~ (Davis and Brewer, 2009). This coincides with the well-ventilated water column
and bottom water in the Gulf of Oman during that time suggesting a response to the obliquity signal.

6 Conclusion

Our study presents a multiproxy approach reconstructing the water column and bottom water oxygenation in the Gulf of Oman
for the past about 43 ka for the first time. The three independent proxies based on bulk sediment ($\delta^{15}N$), lipid biomarker
analysis (ratio of (lycopane + n-C_{35})/n-C_{31}) and benthic foraminifera taxa (Enhanced Benthic Foraminiferal Oxygen
Index~~EBFOI~~ including transfer function of Kranner et al. (2022)) show a robust and mostly consistent pattern in our record.
The Holocene is characterized by strong OMZ conditions and bottom water deoxygenation, which is consistent with other

studies from the Arabian Sea. In contrast to other regions in the Arabian Sea, the water column and the bottom water in the Gulf of Oman were very well ventilated during the LGM/MIS 2. The ~~very~~ well oxygenated ~~ventilated~~ conditions of the Gulf of Oman lead to a highly diverse benthic foraminiferal assemblage. We attribute the good ventilation to stronger wind-induced mixing of the water column and better ventilation by oxygen-richer oceanic currents leading to stronger northward intrusion of the AAIW, corroborating other recent studies. The OMZ strength and bottom water oxygenation reconstruction during MIS 3 reveal oscillating conditions of moderately-oxygenated (stadials) and deoxygenated conditions (interstadials, D/O events). Besides the prominent D/O cycles, we also found prominent high frequency periods (570 to 710 years) during MIS 3 by using spectral and wavelet analyses.

In consideration of our results, we propose two different modes of the oxygenation status for the past about 43 ka. The first mode is a stable period of either strong OMZ and bottom water deoxygenation (Holocene) or well oxygenation of the water column and bottom water (LGM/MIS 2). The second mode is an unstable period with oscillations between moderately oxygenated and deoxygenated conditions, respectively. This is visible in the MIS 3 period of our record with ~~swinging back and forth~~fluctuating high and low oxygen conditions.

Appendix
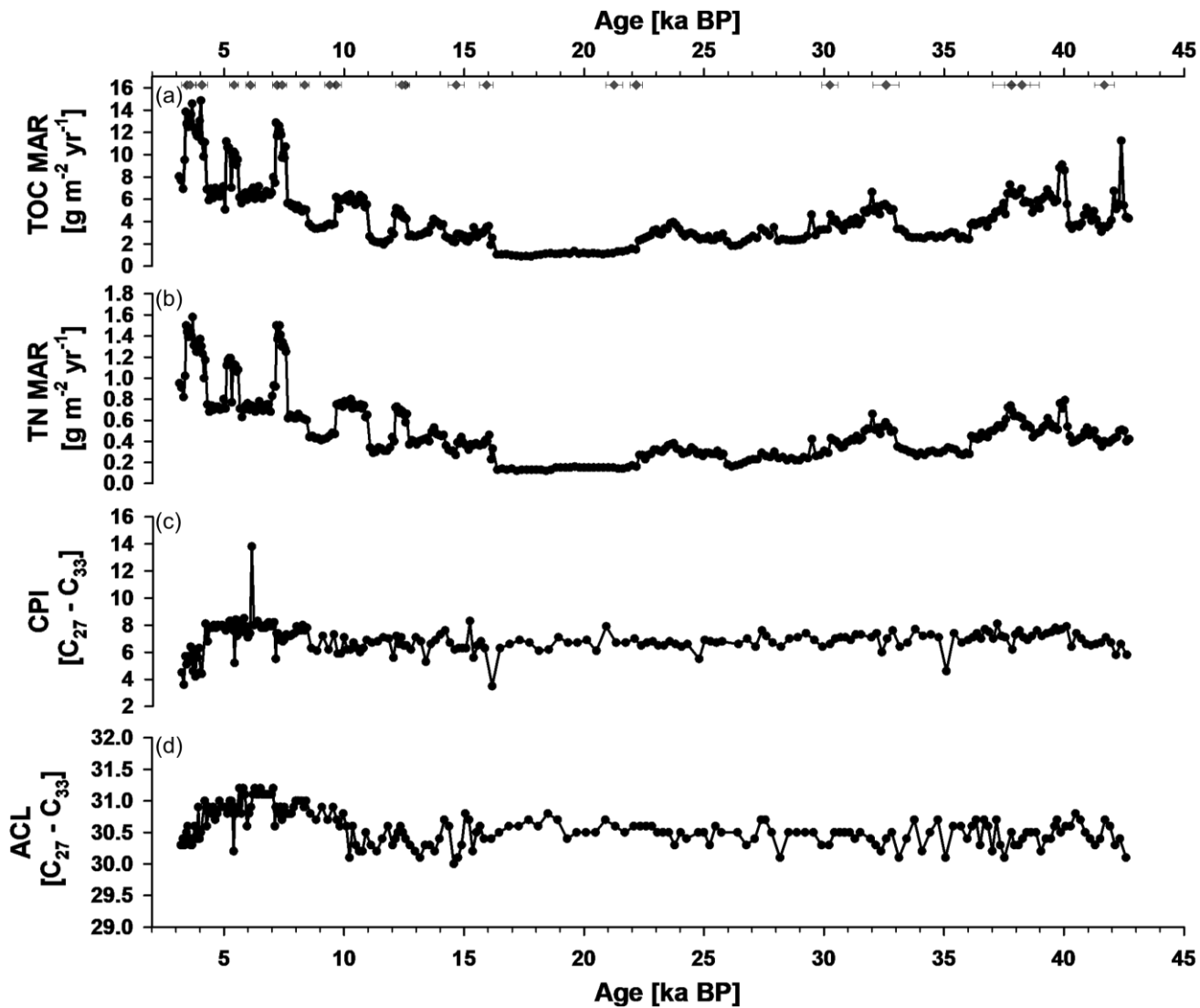
430

Fig. A1: Bulk and plant-wax derived *n*-alkane data of SL167. (a) Total mass accumulation rates of total organic carbon (TOC MAR), (b) total mass accumulation rates of total nitrogen (TN MAR), (c) carbon preference index (CPI) of the *n*-alkanes C_{27} to C_{33} and (ed) average chain length (ACL) of the *n*-alkanes C_{27} to C_{33}. Diamonds showing dated ages of SL167.
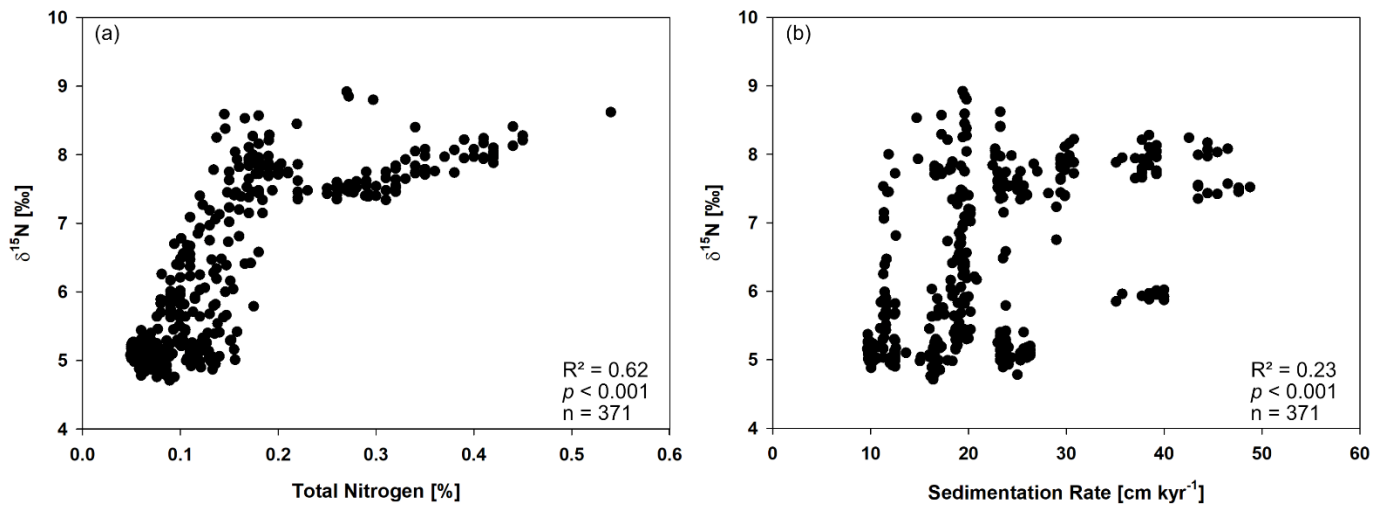
435 **Fig. A2: Crossplots of (a) total nitrogen (TN) and δ¹⁵N as well as (b) the sedimentation rate and δ¹⁵N of sediment core SL167.**

Data availability

The data sets are ~~uploaded to PANGAEA and will be available upon publication~~stored and available at PANGAEA under https://doi.pangaea.de/10.1594/PANGAEA.964226 and https://doi.org/10.1594/PANGAEA.960060 (census date of benthic
440 foraminifera).

Author contributions

NB: conceptualization, formal analysis, investigation, methodology, visualization, writing – original draft preparation. GS: conceptualization, faunal analysis, investigation, methodology, visualization, resources, supervision, writing – original draft preparation. BG: conceptualization, writing – original draft preparation. HS: faunal analysis, writing – original draft
445 preparation. PM: faunal analysis, writing – original draft preparation.

Competing interests

The contact author has declared that none of the authors has any competing interests.

Acknowledgements

This work is funded by the Deutsche Forschungsgemeinschaft (DFG, German Research Foundation) under Germany's Excellence Strategy – EXC 2037 'CLICCS - Climate, Climatic Change, and Society' – Project Number: 390683824, contribution to the Center for Earth System Research and Sustainability (CEN) of Universität Hamburg. Chlorophyll a analyses and visualizations used in this paper were produced with the Giovanni online data system, developed and maintained by the NASA GES DISC. We also acknowledge the MODIS mission scientists and associated NASA personnel for the production of the data used in this research effort. We thank Frauke Langenberg, Marc Metzke, Miriam Warning, Jan Maier, Dorothea Bunzel, Tobias Winkler and Sabine Beckmann for technical and analytical support. We also thank the two anonymous reviewer for their constructive comments and improving the manuscript.

References

Acharya, S. S. and Panigrahi, M. K.: Eastward shift and maintenance of Arabian Sea oxygen minimum zone: Understanding the paradox, Deep Sea Res. Part I Oceanogr. Res. Pap., 115, 240–252, doi:10.1016/j.dsr.2016.07.004, 2016.

Allard, J. L., Hughes, P. D. and Woodward, J. C.: Heinrich Stadial aridity forced Mediterranean-wide glacier retreat in the last cold stage, Nat. Geosci., 14(4), 197–205, doi:10.1038/s41561-021-00703-6, 2021.

Altabet, M. A., Francois, R., Murray, D. W. and Prell, W. L.: Climate-related variations in denitrification in the Arabian Sea from sediment 15N/14N ratios, Nature, 373(6514), 506–509, doi:10.1038/373506a0, 1995.

Altabet, M. A., Pilskaln, C., Thunell, R., Pride, C., Sigman, D., Chavez, F. and Francois, R.: The nitrogen isotope biogeochemistry of sinking particles from the margin of the Eastern North Pacific, Deep Sea Res. Part I Oceanogr. Res. Pap., 46(4), 655–679, doi:https://doi.org/10.1016/S0967-0637(98)00084-3, 1999.

Altabet, M. A., Higginson, M. J. and Murray, D. W.: The effect of millennial-scale changes in Arabian Sea denitrification on atmospheric CO2, Nature, 415(6868), 159–162, doi:10.1038/415159a, 2002.

Andruleit, H., Stäger, S., Rogalla, U. and Cepek, P.: Living coccolithophores in the northern Arabian Sea: Ecological tolerances and environmental control, Mar. Micropaleontol., 49(1–2), 157–181, doi:10.1016/S0377-8398(03)00049-5, 2003.

Arz, H. W., Lamy, F., Ganopolski, A., Nowaczyk, N. and Pätzold, J.: Dominant Northern Hemisphere climate control over millennial-scale glacial sea-level variability, Quat. Sci. Rev., 26(3), 312–321, doi:https://doi.org/10.1016/j.quascirev.2006.07.016, 2007.

Beal, L. M., Ffield, A. and Gordon, A. L.: Spreading of Red Sea overflow waters in the Indian Ocean, J. Geophys. Res. Ocean., 105(C4), 8549–8564, doi:https://doi.org/10.1029/1999JC900306, 2000.

van Bentum, E. C., Hetzel, A., Brumsack, H.-J., Forster, A., Reichart, G.-J. and Sinninghe Damsté, J. S.: Reconstruction of water column anoxia in the equatorial Atlantic during the Cenomanian–Turonian oceanic anoxic event using biomarker and trace metal proxies, Palaeogeogr. Palaeoclimatol. Palaeoecol., 280(3), 489–498, doi:https://doi.org/10.1016/j.palaeo.2009.07.003, 2009.

480   Blaauw, M. and Christen, J. A.: Flexible paleoclimate age-depth models using an autoregressive gamma process, Bayesian Anal., 6(3), 457–474, doi:10.1214/11-BA618, 2011.

Böll, A., Lückge, A., Munz, P., Forke, S., Schulz, H., Ramaswamy, V., Rixen, T., Gaye, B. and Emeis, K. C.: Late Holocene primary productivity and sea surface temperature variations in the northeastern Arabian Sea: Implications for winter monsoon variability, Paleoceanography, 29, 778–794, doi:10.1002/2013PA002579, 2014.

485   Bond, G., Kromer, B., Beer, J., Muscheler, R., Evans, M. N., Showers, W., Hoffmann, S., Lotti-Bond, R., Hajdas, I. and Bonani, G.: Persistent solar influence on North Atlantic climate during the Holocene., Science, 294, 2130–2136, doi:10.1126/science.1065680, 2001.

Bopp, L., Resplandy, L., Orr, J. C., Doney, S. C., Dunne, J. P., Gehlen, M., Halloran, P., Heinze, C., Ilyina, T., Séférian, R., Tjiputra, J. and Vichi, M.: Multiple stressors of ocean ecosystems in the 21st century: projections with CMIP5 models,
490   Biogeosciences, 10(10), 6225–6245, doi:10.5194/bg-10-6225-2013, 2013.

Bower, A. S., Hunt, H. D. and Price, J. F.: Character and dynamics of the Red Sea and Persian Gulf outflows, J. Geophys. Res. Ocean., 105(C3), 6387–6414, doi:https://doi.org/10.1029/1999JC900297, 2000.

Bray, E. . and Evans, E. .: Distribution of n-paraffins as a clue to recognition of source beds, Geochim. Cosmochim. Acta, 22(1), 2–15, doi:10.1016/0016-7037(61)90069-2, 1961.

495   Breitburg, D., Levin, L. A., Oschlies, A., Grégoire, M., Chavez, F. P., Conley, D. J., Garçon, V., Gilbert, D., Gutiérrez, D., Isensee, K., Jacinto, G. S., Limburg, K. E., Montes, I., Naqvi, S. W. A., Pitcher, G. C., Rabalais, N. N., Roman, M. R., Rose, K. A., Seibel, B. A., Telszewski, M., Yasuhara, M. and Zhang, J.: Declining oxygen in the global ocean and coastal waters, Science (80-.)., 359(6371), eaam7240, doi:10.1126/science.aam7240, 2018.

Bronough, D.: ncdf4.helpers: Helper Functions for Use with the "ncdf4" Package, [online] Available from: https://cran.r-
500   project.org/package=ncdf4.helpers, 2021.

Buizert, C. and Schmittner, A.: Southern Ocean control of glacial AMOC stability and Dansgaard-Oeschger interstadial duration, Paleoceanography, 30(12), 1595–1612, doi:https://doi.org/10.1002/2015PA002795, 2015.

Bunn, A., Korpela, M., Biondi, F., Campelo, F., Mérian, P., Qeadan, F. and Zang, C.: dplR: Dendrochronology Program Library in R, [online] Available from: https://cran.r-project.org/package=dplR, 2022.

505   Bunn, A. G.: A dendrochronology program library in R (dplR), Dendrochronologia, 26(2), 115–124, doi:https://doi.org/10.1016/j.dendro.2008.01.002, 2008.

Bunn, A. G.: Statistical and visual crossdating in R using the dplR library, Dendrochronologia, 28(4), 251–258, doi:https://doi.org/10.1016/j.dendro.2009.12.001, 2010.

Burdanowitz, N., Gaye, B., Hilbig, L., Lahajnar, N., Lückge, A., Rixen, T. and Emeis, K. C.: Holocene monsoon and sea level-
510   related changes of sedimentation in the northeastern Arabian Sea, Deep. Res. Part II Top. Stud. Oceanogr., 166, 6–18, doi:10.1016/j.dsr2.2019.03.003, 2019.

Burdanowitz, N., Rixen, T., Gaye, B. and Emeis, K.-C.: Signals of Holocene climate transition amplified by anthropogenic land-use changes in the westerly--Indian monsoon realm, Clim. Past, 17(4), 1735–1749, doi:10.5194/cp-17-1735-2021, 2021.

Busecke, J. J. M., Resplandy, L., Ditkovsky, S. J. and John, J. G.: Diverging Fates of the Pacific Ocean Oxygen Minimum

515   Zone and Its Core in a Warming World, AGU Adv., 3(6), e2021AV000470, doi:https://doi.org/10.1029/2021AV000470, 2022.

Bush, R. T. and McInerney, F. A.: Leaf wax *n*-alkane distributions in and across modern plants: Implications for paleoecology

and chemotaxonomy, Geochim. Cosmochim. Acta, 117, 161–179, doi:10.1016/j.gca.2013.04.016, 2013.

Buzas, M. A. and Gibson, T. G.: Species Diversity: Benthonic Foraminifera in Western North Atlantic, Science (80-.).,

163(3862), 72–75, doi:10.1126/science.163.3862.72, 1969.

520   Carr, A. S., Boom, A., Grimes, H. L., Chase, B. M., Meadows, M. E. and Harris, A.: Leaf wax *n*-alkane distributions in arid

zone South African flora: Environmental controls, chemotaxonomy and palaeoecological implications, Org. Geochem., 67,

72–84, doi:10.1016/j.orggeochem.2013.12.004, 2014.

Casciotti, K. L.: Nitrogen and Oxygen Isotopic Studies of the Marine Nitrogen Cycle, Ann. Rev. Mar. Sci., 8(1), 379–407,

doi:10.1146/annurev-marine-010213-135052, 2016.

525   Clift, P. D. and Plumb, R. A.: The Asian Monsoon: Causes, History and Effects, Cambridge University Press, Cambridge.,

2008.

Collister, J. W., Rieley, G., Stern, B., Eglinton, G. and Fry, B.: Compound-specific δ 13C analyses of leaf lipids from plants

with differing carbon dioxide metabolisms, Org. Geochem., 21(6–7), 619–627, doi:10.1016/0146-6380(94)90008-6, 1994.

Cooper, R. J., Pedentchouk, N., Hiscock, K. M., Disdle, P., Krueger, T. and Rawlins, B. G.: Apportioning sources of organic

530   matter in streambed sediments: An integrated molecular and compound-specific stable isotope approach, Sci. Total Environ.,

520, 187–197, doi:10.1016/j.scitotenv.2015.03.058, 2015.

Cranwell, P. A.: Extractable and bound lipid components in a freshwater sediment, Geochim. Cosmochim. Acta, 42(10), 1523–

1532, doi:https://doi.org/10.1016/0016-7037(78)90023-6, 1978.

Cranwell, P. A.: Diagenesis of free and bound lipids in terrestrial detritus deposited in a lacustrine sediment, Org. Geochem.,

535   3(3), 79–89 [online] Available from: http://www.sciencedirect.com/science/article/pii/0146638081900024 (Accessed 20

January 2014), 1981.

Cullen, H. M., DeMenocal, P. B., Hemming, S., Hemming, G., Brown, F. H., Guilderson, T. and Sirocko, F.: Climate change

and the collapse of the Akkadian empire: Evidence from the deep sea, Geology, 28(4), 379–382, doi:10.1130/0091-

7613(2000)28<379:CCATCO>2.0.CO;2, 2000.

540   Davis, B. A. S. and Brewer, S.: Orbital forcing and role of the latitudinal insolation/temperature gradient, Clim. Dyn., 32(2–

3), 143–165, doi:10.1007/s00382-008-0480-9, 2009.

Debenay, J.-P.: A Guide to 1,000 Foraminifera from Southwestern Pacific, New Caledonia, Publications Scientifiques du

Muséum, Muséum national d'Histoire naturelle, Paris., 2012.

Deplazes, G., Lückge, A., Peterson, L. C., Timmermann, A., Hamann, Y., Hughen, K. A., Röhl, U., Laj, C., Cane, M. A.,

545   Sigman, D. M. and Haug, G. H.: Links between tropical rainfall and North Atlantic climate during the last glacial period, Nat.

Geosci., 6(3), 213–217, doi:10.1038/ngeo1712, 2013.

Deplazes, G., Lückge, A., Stuut, J. B. W., Pätzold, J., Kuhlmann, H., Husson, D., Fant, M. and Haug, G. H.: Weakening and

strengthening of the Indian monsoon during Heinrich events and Dansgaard-Oeschger oscillations, Paleoceanography, 29(2), 99–114, doi:10.1002/2013PA002509, 2014.

550 Den Dulk, M.: Benthic foraminiferal response to Late Quaternary variations in surface water productivity and oxygenation in the northern Arabian Sea, Geol. Ultraiectina, 188, 1–205, 2000.

Dummann, W., Steinig, S., Hofmann, P., Lenz, M., Kusch, S., Flögel, S., Herrle, J. O., Hallmann, C., Rethemeyer, J., Kasper, H. U. and Wagner, T.: Driving mechanisms of organic carbon burial in the Early Cretaceous South Atlantic Cape Basin (DSDP Site 361), Clim. Past, 17(1), 469–490, doi:10.5194/cp-17-469-2021, 2021.

555 Dutt, S., Gupta, A. K., Clemens, S. C., Cheng, H., Singh, R. K., Kathayat, G. and Edwards, R. L.: Abrupt changes in Indian summer monsoon strength during 33,800 to 5500 years B.P., Geophys. Res. Lett., 42(13), 5526–5532, doi:https://doi.org/10.1002/2015GL064015, 2015.

Eglinton, G. and Hamilton, R.: Leaf epicuticular waxes, Science, 156(3780), 1322–1335, 1967.

Eglinton, T. I. and Eglinton, G.: Molecular proxies for paleoclimatology, Earth Planet. Sci. Lett., 275(1–2), 1–16, 560 doi:10.1016/j.epsl.2008.07.012, 2008.

Farrington, J. W., Davis, A. C., Sulanowski, J., McCaffrey, M. A., McCarthy, M., Clifford, C. H., Dickinson, P. and Volkman, J. K.: Biogeochemistry of lipids in surface sediments of the Peru Upwelling Area at 15°S, Org. Geochem., 13(4), 607–617, doi:https://doi.org/10.1016/0146-6380(88)90080-0, 1988.

Fleitmann, D., Cheng, H., Badertscher, S., Edwards, R. L., Mudelsee, M., Göktürk, O. M., Fankhauser, A., Pickering, R., 565 Raible, C. C., Matter, A., Kramers, J. and Tüysüz, O.: Timing and climatic impact of Greenland interstadials recorded in stalagmites from northern Turkey, Geophys. Res. Lett., 36(19), doi:https://doi.org/10.1029/2009GL040050, 2009.

Fontanier, C., Jorissen, F. J., Licari, L., Alexandre, A., Anschutz, P. and Carbonel, P.: Live benthic foraminiferal faunas from the Bay of Biscay: faunal density, composition, and microhabitats, Deep Sea Res. Part I Oceanogr. Res. Pap., 49(4), 751–785, doi:https://doi.org/10.1016/S0967-0637(01)00078-4, 2002.

570 Freeman, K. H., Wakeham, S. G. and Hayes, J. M.: Predictive isotopic biogeochemistry: Hydrocarbons from anoxic marine basins, Org. Geochem., 21(6), 629–644, doi:https://doi.org/10.1016/0146-6380(94)90009-4, 1994.

Friederich, G. E., Ledesma, J., Ulloa, O. and Chavez, F. P.: Air–sea carbon dioxide fluxes in the coastal southeastern tropical Pacific, Prog. Oceanogr., 79(2), 156–166, doi:https://doi.org/10.1016/j.pocean.2008.10.001, 2008.

Gaye-Haake, B., Lahajnar, N., Emeis, K. C., Unger, D., Rixen, T., Suthhof, A., Ramaswamy, V., Schulz, H., Paropkari, A. L., 575 Guptha, M. V. S. and Ittekkot, V.: Stable nitrogen isotopic ratios of sinking particles and sediments from the northern Indian Ocean, Mar. Chem., 96(3–4), 243–255, doi:10.1016/j.marchem.2005.02.001, 2005.

Gaye, B., Böll, A., Segschneider, J., Burdanowitz, N., Emeis, K.-C., Ramaswamy, V., Lahajnar, N., Lückge, A. and Rixen, T.: Glacial--interglacial changes and Holocene variations in Arabian Sea denitrification, Biogeosciences, 15(2), 507–527, doi:10.5194/bg-15-507-2018, 2018.

580 Gooday, A. J. B. T.: Benthic foraminifera (protista) as tools in deep-water palaeoceanography: Environmental influences on faunal characteristics, Adv. Mar. Biol., 46, 1–90, doi:https://doi.org/10.1016/S0065-2881(03)46002-1, 2003.

Gouhier, T. C., Grinsted, A. and Simko, V.: R package {biwavelet}: Conduct Univariate and Bivariate Wavelet Analyses, [online] Available from: https://github.com/tgouhier/biwavelet, 2021.

Gruber, N.: The Dynamics of the Marine Nitrogen Cycle and its Influence on Atmospheric CO2 Variations, edited by M. Follows and T. Oguz, pp. 97–148, Springer Netherlands, Dordrecht., 2004.

Haake, B., Ittekkot, V., Rixen, T., Ramaswamy, V., Nair, R. R. and Curry, W. B.: Seasonality and interannual variability of particle fluxes to the deep Arabian sea, Deep. Res. Part I, 40(7), 1323–1344, doi:10.1016/0967-0637(93)90114-I, 1993.

Helly, J. J. and Levin, L. A.: Global distribution of naturally occurring marine hypoxia on continental margins, Deep Sea Res. Part I Oceanogr. Res. Pap., 51(9), 1159–1168, doi:https://doi.org/10.1016/j.dsr.2004.03.009, 2004.

Herrmann, N., Boom, A., Carr, A. S., Chase, B. M., Granger, R., Hahn, A., Zabel, M. and Schefuß, E.: Sources, transport and deposition of terrestrial organic material: A case study from southwestern Africa, Quat. Sci. Rev., 149, 215–229, doi:10.1016/j.quascirev.2016.07.028, 2016.

Hunt, K. M. R., Turner, A. G. and Shaffrey, L. C.: The evolution, seasonality and impacts of western disturbances, Q. J. R. Meteorol. Soc., 144(710), 278–290, doi:10.1002/qj.3200, 2018.

Ivanochko, T. S., Ganeshram, R. S., Brummer, G.-J. A., Ganssen, G., Jung, S. J. A., Moreton, S. G. and Kroon, D.: Variations in tropical convection as an amplifier of global climate change at the millennial scale, Earth Planet. Sci. Lett., 235(1), 302–314, doi:https://doi.org/10.1016/j.epsl.2005.04.002, 2005.

Jaglan, S., Gupta, A. K., Clemens, S. C., Dutt, S., Cheng, H. and Singh, R. K.: Abrupt Indian summer monsoon shifts aligned with Heinrich events and D-O cycles since MIS 3, Palaeogeogr. Palaeoclimatol. Palaeoecol., 583, 110658, doi:https://doi.org/10.1016/j.palaeo.2021.110658, 2021.

Jones, R. W.: The Challenger Foraminifera, Oxford University Press, Oxford., 1994.

Jorissen, F. J., de Stigter, H. C. and Widmark, J. G. V: A conceptual model explaining benthic foraminiferal microhabitats, Mar. Micropaleontol., 26(1), 3–15, doi:https://doi.org/10.1016/0377-8398(95)00047-X, 1995.

Jung, M., Ilmberger, J., Mangini, A. and Emeis, K.-C.: Why some Mediterranean sapropels survived burn-down (and others did not), Mar. Geol., 141(1), 51–60, doi:https://doi.org/10.1016/S0025-3227(97)00031-5, 1997.

Jung, S. J. A., Kroon, D., Ganssen, G., Peeters, F. and Ganeshram, R.: Enhanced Arabian Sea intermediate water flow during glacial North Atlantic cold phases., 2009.

Junium, C. K., Arthur, M. A. and Freeman, K. H.: Compound-specific δ15N and chlorin preservation in surface sediments of the Peru Margin with implications for ancient bulk δ15N records, Geochim. Cosmochim. Acta, 160, 306–318, doi:https://doi.org/10.1016/j.gca.2014.12.018, 2015.

Kessarkar, P. M., Purnachadra Rao, V., Naqvi, S. W. A. and Karapurkar, S. G.: Variation in the Indian summer monsoon intensity during the Bølling-Ållerød and Holocene, Paleoceanography, 28(3), 413–425, doi:10.1002/palo.20040, 2013.

Koho, K. A., García, R., de Stigter, H. C., Epping, E., Koning, E., Kouwenhoven, T. J. and van der Zwaan, G. J.: Sedimentary labile organic carbon and pore water redox control on species distribution of benthic foraminifera: A case study from Lisbon–Setúbal Canyon (southern Portugal), Prog. Oceanogr., 79(1), 55–82, doi:https://doi.org/10.1016/j.pocean.2008.07.004, 2008.

Kranner, M., Harzhauser, M., Beer, C., Auer, G. and Piller, W. E.: Calculating dissolved marine oxygen values based on an enhanced Benthic Foraminifera Oxygen Index, Sci. Rep., 12(1), 1376, doi:10.1038/s41598-022-05295-8, 2022.

Kumar, S. P. and Prasad, T. G.: Formation and spreading of Arabian Sea high-salinity water mass, J. Geophys. Res. Ocean., 104(C1), 1455–1464, doi:https://doi.org/10.1029/1998JC900022, 1999.

620   Kuniyoshi, Y., Abe-Ouchi, A., Sherriff-Tadano, S., Chan, W.-L. and Saito, F.: Effect of Climatic Precession on Dansgaard-Oeschger-Like Oscillations, Geophys. Res. Lett., 49(6), e2021GL095695, doi:https://doi.org/10.1029/2021GL095695, 2022.

L'Hégaret, P., Duarte, R., Carton, X., Vic, C., Ciani, D., Baraille, R. and Corréard, S.: Mesoscale variability in the Arabian Sea from HYCOM model results and observations: impact on the Persian Gulf Water path, Ocean Sci., 11(5), 667–693, doi:10.5194/os-11-667-2015, 2015.

625   Lachkar, Z., Lévy, M. and Smith, K. S.: Strong Intensification of the Arabian Sea Oxygen Minimum Zone in Response to Arabian Gulf Warming, Geophys. Res. Lett., 46(10), 5420–5429, doi:https://doi.org/10.1029/2018GL081631, 2019.

Lambeck, K.: Shoreline reconstructions for the Persian Gulf since the last glacial maximum, Earth Planet. Sci. Lett., 142(1–2), 43–57, doi:10.1016/0012-821x(96)00069-6, 1996.

Lauterbach, S., Witt, R., Plessen, B., Dulski, P., Prasad, S., Mingram, J., Gleixner, G., Hettler-Riedel, S., Stebich, M.,
630   Schnetger, B., Schwalb, A. and Schwarz, A.: Climatic imprint of the mid-latitude Westerlies in the Central Tian Shan of Kyrgyzstan and teleconnections to North Atlantic climate variability during the last 6000 years, The Holocene, 24(8), 970–984, doi:10.1177/0959683614534741, 2014.

Lemieux-Dudon, B., Blayo, E., Petit, J.-R., Waelbroeck, C., Svensson, A., Ritz, C., Barnola, J.-M., Narcisi, B. M. and Parrenin, F.: Consistent dating for Antarctic and Greenland ice cores, Quat. Sci. Rev., 29(1), 8–20,
635   doi:https://doi.org/10.1016/j.quascirev.2009.11.010, 2010.

Leuschner, D. C. and Sirocko, F.: The low-latitude monsoon climate during Dansgaard–Oeschger cycles and Heinrich Events, Quat. Sci. Rev., 19(1), 243–254, doi:https://doi.org/10.1016/S0277-3791(99)00064-5, 2000.

Levin, L. A.: Oxygen minimum zone Benthos: Adaptation and community response to hypoxia, Oceanogr. Mar. Biol., 41, 1–45 [online] Available from: https://api.semanticscholar.org/CorpusID:85701346, 2003.

640   Liu, H. Y., Lin, Z. S., Qi, X. Z., Li, Y. X., Yu, M. T., Yang, H. and Shen, J.: Possible link between Holocene East Asian monsoon and solar activity obtained from the EMD method, Nonlinear Process. Geophys., 19(4), 421–430, doi:10.5194/npg-19-421-2012, 2012.

Lu, W., Costa, K. M. and Oppo, D. W.: Reconstructing the Oxygen Depth Profile in the Arabian Sea During the Last Glacial Period, Paleoceanogr. Paleoclimatology, 38(6), doi:10.1029/2023pa004632, 2023.

645   Madhupratap, M., Kumar, S. P., Bhattathiri, P. M. A., Kumar, M. D., Raghukumar, S., Nair, K. K. C. and Ramaiah, N.: Mechanism of the biological response to winter cooling in the northeastern Arabian Sea, Nature, 384(6609), 549–552, doi:10.1038/384549a0, 1996.

de Marez, C., L'Hégaret, P., Morvan, M. and Carton, X.: On the 3D structure of eddies in the Arabian Sea, Deep Sea Res. Part I Oceanogr. Res. Pap., 150, 103057, doi:https://doi.org/10.1016/j.dsr.2019.06.003, 2019.

650 Menzel, P., Gaye, B., Mishra, P. K., Anoop, A., Basavaiah, N., Marwan, N., Plessen, B., Prasad, S., Riedel, N., Stebich, M. and Wiesner, M. G.: Linking Holocene drying trends from Lonar Lake in monsoonal central India to North Atlantic cooling events, Palaeogeogr. Palaeoclimatol. Palaeoecol., 410, 164–178, doi:10.1016/j.palaeo.2014.05.044, 2014.

Meyers, P. A. and Ishiwatari, R.: Lacustrine organic geochemistry—an overview of indicators of organic matter sources and diagenesis in lake sediments, Org. Geochem., 20(7), 867–900, doi:10.1016/0146-6380(93)90100-P, 1993.

655 Möbius, J., Gaye, B., Lahajnar, N., Bahlmann, E. and Emeis, K.-C.: Influence of diagenesis on sedimentary $\delta 15N$ in the Arabian Sea over the last 130kyr, Mar. Geol., 284(1), 127–138, doi:10.1016/j.margeo.2011.03.013, 2011.

Montoya, J. P.: Nitrogen Stable Isotopes in Marine Environments, in Nitrogen in the Marine Environment, edited by D. G. Capone, D. A. Bronk, M. R. Mulholland, and E. J. B. T.-N. in the M. E. (Second E. Carpenter, pp. 1277–1302, Academic Press, San Diego., 2008.

660 Morrison, J. M., Codispoti, L. A., Gaurin, S., Jones, B., Manghnani, V. and Zheng, Z.: Seasonal variation of hydrographic and nutrient fields during the US JGOFS Arabian Sea Process Study, Deep Sea Res. Part II Top. Stud. Oceanogr., 45(10), 2053–2101, doi:https://doi.org/10.1016/S0967-0645(98)00063-0, 1998.

Munz, P. M., Steinke, S., Böll, A., Lückge, A., Groeneveld, J., Kucera, M. and Schulz, H.: Decadal resolution record of Oman upwelling indicates solar forcing of the Indian summer monsoon (9--6\,ka), Clim. Past, 13(5), 491–509, doi:10.5194/cp-13-665 491-2017, 2017.

Murray, J. W.: Ecology and palaeoecology of benthic foraminifera, Longman Scientific & Technical, New York., 1991.

Naeher, S., Geraga, M., Papatheodorou, G., Ferentinos, G., Kaberi, H. and Schubert, C. J.: Environmental variations in a semi-enclosed embayment (Amvrakikos Gulf, Greece) – reconstructions based on benthic foraminifera abundance and lipid biomarker pattern, Biogeosciences, 9(12), 5081–5094, doi:10.5194/bg-9-5081-2012, 2012.

670 Naqvi, S. W. A., Bange, H. W., Far\'\ias, L., Monteiro, P. M. S., Scranton, M. I. and Zhang, J.: Marine hypoxia/anoxia as a source of CH4 and N2O, Biogeosciences, 7(7), 2159–2190, doi:10.5194/bg-7-2159-2010, 2010.

NASA: Moderate-resolution Imaging Spectroradiometer (MODIS) Aqua Chlorophyll Data, , doi:doi: 10.5067/AQUA/MODIS/L3M/CHL/2022, 2022.

Neff, U., Burns, S. J., Mangini, A., Mudelsee, M., Fleitmann, D. and Matter, A.: Strong coherence between solar variability 675 and the monsoon in Oman between 9 and 6 kyr ago, Nature, 411(6835), 290–293, doi:10.1038/35077048, 2001.

North Greenland Ice Core Project members: High-resolution record of Northern Hemisphere climate extending into the last interglacial period, Nature, 431(7005), 147–151, doi:10.1038/nature02805, 2004.

Obrochta, S. P., Miyahara, H., Yokoyama, Y. and Crowley, T. J.: A re-examination of evidence for the North Atlantic " 1500-year cycle" at Site 609, Quat. Sci. Rev., 55, 23–33, doi:10.1016/j.quascirev.2012.08.008, 2012.

680 Ogihara, S.: Is the lycopane/n-C31ratio an effective proxy of palaeoxicity of bottom water for the Japan Sea? - Unusual distribution of lycopane in the surface sediment from the Japan Sea collected by the MD179 cruise, J. Asian Earth Sci., 90, 250–253, doi:10.1016/j.jseaes.2013.12.012, 2014.

Orsi, W. D., Coolen, M. J. L., Wuchter, C., He, L., More, K. D., Irigoien, X., Chust, G., Johnson, C., Hemingway, J. D., Lee,

M., Galy, V. and Giosan, L.: Climate oscillations reflected within the microbiome of Arabian Sea sediments, Sci. Rep., 7(1),

685   6040, doi:10.1038/s41598-017-05590-9, 2017.

Overpeck, J., Anderson, D., Trumbore, S. and Prell, W.: The southwest Indian Monsoon over the last 18000 years, Clim. Dyn., 12(3), 213–225, doi:10.1007/BF00211619, 1996.

Pahnke, K. and Zahn, R.: Southern Hemisphere Water Mass Conversion Linked with North Atlantic Climate Variability, Science (80-.)., 307(5716), 1741–1746, doi:10.1126/science.1102163, 2005.

690   Pancost, R. D. and Boot, C. S.: The palaeoclimatic utility of terrestrial biomarkers in marine sediments, Mar. Chem., 92(1), 239–261, doi:https://doi.org/10.1016/j.marchem.2004.06.029, 2004.

Pathak, V. K., Kharwar, A. and Rai, A. K.: Benthic foraminiferal response to changes in the northwestern Arabian Sea oxygen minimum zone (OMZ) during past ~145 kyr, J. Earth Syst. Sci., 130(3), 163, doi:10.1007/s12040-021-01659-2, 2021.

Paulmier, A. and Ruiz-Pino, D.: Oxygen minimum zones (OMZs) in the modern ocean, Prog. Oceanogr., 80(3), 113–128,

695   doi:https://doi.org/10.1016/j.pocean.2008.08.001, 2009.

Paulmier, A., Ruiz-Pino, D. and Garçon, V.: CO2 maximum in the oxygen minimum zone (OMZ), Biogeosciences, 8(2), 239–252, doi:10.5194/bg-8-239-2011, 2011.

Pichevin, L., Bard, E., Martinez, P. and Billy, I.: Evidence of ventilation changes in the Arabian Sea during the late Quaternary: Implication for denitrification and nitrous oxide emission, Global Biogeochem. Cycles, 21(4), n/a-n/a,

700   doi:10.1029/2006GB002852, 2007.

Pous, S. P., Carton, X. and Lazure, P.: Hydrology and circulation in the Strait of Hormuz and the Gulf of Oman—Results from the GOGP99 Experiment: 2. Gulf of Oman, J. Geophys. Res. Ocean., 109(C12), doi:https://doi.org/10.1029/2003JC002146, 2004.

Prasad, T. G., Ikeda, M. and Kumar, S. P.: Seasonal spreading of the Persian Gulf Water mass in the Arabian Sea, J. Geophys.

705   Res. Ocean., 106(C8), 17059–17071, doi:https://doi.org/10.1029/2000JC000480, 2001.

R Core Team: R: A Language and Environment for Statistical Computing, [online] Available from: https://www.r-project.org/, 2023.

von Rad, U., Schaaf, M., Michels, K. H., Schulz, H., Berger, W. H. and Sirocko, F.: A 5000-yr Record of Climate Change in Varved Sediments from the Oxygen Minimum Zone off Pakistan, Northeastern Arabian Sea, Quat. Res., 51(1), 39–53,

710   doi:10.1006/qres.1998.2016, 1999.

Reichart, G. J., den Dulk, M., Visser, H. J., van der Weijden, C. H. and Zachariasse, W. J.: A 225 kyr record of dust supply, paleoproductivity and the oxygen minimum zone from the Murray Ridge (northern Arabian Sea), Palaeogeogr. Palaeoclimatol. Palaeoecol., 134(1), 149–169, doi:http://dx.doi.org/10.1016/S0031-0182(97)00071-0, 1997.

Reichart, G. J., Lourens, L. J. and Zachariasse, W. J.: Temporal variability in the northern Arabian Sea oxygen minimum zone

715   (OMZ) during the last 225,000 years, Paleoceanography, 13(6), 607–621, doi:10.1029/98PA02203, 1998.

Reimer, P. J. and Reimer, R. W.: A Marine Reservoir Correction Database and On-Line Interface, Radiocarbon, 43(2A), 461–463, doi:DOI: 10.1017/S0033822200038339, 2001.

Rixen, T., Baum, A., Gaye, B. and Nagel, B.: Seasonal and interannual variations in the nitrogen cycle in the Arabian Sea, Biogeosciences, 11(20), 5733–5747, doi:10.5194/bg-11-5733-2014, 2014.

720 Rixen, T., Cowie, G., Gaye, B., Goes, J., do Rosário Gomes, H., Hood, R. R., Lachkar, Z., Schmidt, H., Segschneider, J. and Singh, A.: Reviews and syntheses: Present, past, and future of the oxygen minimum zone in the northern Indian Ocean, Biogeosciences, 17(23), 6051–6080, doi:10.5194/bg-17-6051-2020, 2020.

Rohling, E. J., Grant, K., Hemleben, C., Kucera, M., Roberts, A. P., Schmeltzer, I., Schulz, H., Siccha, M., Siddall, M. and Trommer, G.: New constraints on the timing of sea level fluctuations during early to middle marine isotope stage 3, 725 Paleoceanography, 23(3), doi:https://doi.org/10.1029/2008PA001617, 2008.

Rommerskirchen, F., Plader, A., Eglinton, G., Chikaraishi, Y. and Rullkötter, J.: Chemotaxonomic significance of distribution and stable carbon isotopic composition of long-chain alkanes and alkan-1-ols in C4 grass waxes, Org. Geochem., 37(10), 1303–1332, doi:10.1016/j.orggeochem.2005.12.013, 2006.

Russell, J. M. and Johnson, T. C.: Late Holocene climate change in the North Atlantic and equatorial Africa: Millennial-scale 730 ITCZ migration, Geophys. Res. Lett., 32(17), 1–4, doi:10.1029/2005GL023295, 2005.

Russell, J. M., Johnson, T. C. and Talbot, M. R.: A 725 yr cycle in the climate of central Africa during the late Holocene, Geology, 31(8), 677–680, doi:10.1130/G19449.1, 2003.

Sabino, M., Schefuß, E., Natalicchio, M., Dela Pierre, F., Birgel, D., Bortels, D., Schnetger, B. and Peckmann, J.: Climatic and hydrologic variability in the northern Mediterranean across the onset of the Messinian salinity crisis, Palaeogeogr. 735 Palaeoclimatol. Palaeoecol., 545, 109632, doi:https://doi.org/10.1016/j.palaeo.2020.109632, 2020.

Sabino, M., Dela Pierre, F., Natalicchio, M., Birgel, D., Gier, S. and Peckmann, J.: The response of water column and sedimentary environments to the advent of the Messinian salinity crisis: insights from an onshore deep-water section (Govone, NW Italy), Geol. Mag., 158(5), 825–841, doi:DOI: 10.1017/S0016756820000874, 2021.

Saravanan, P., Gupta, A. K., Zheng, H., Majumder, J., Panigrahi, M. K. and Kharya, A.: A 23000 year old record of 740 paleoclimatic and environmental changes from the eastern Arabian Sea, Mar. Micropaleontol., 160, 101905, doi:https://doi.org/10.1016/j.marmicro.2020.101905, 2020.

Sarkar, A., Ramesh, R., Somayajulu, B. L. K., Agnihotri, R., Jull, A. J. T. and Burr, O. S.: High resolution Holocene monsoon record from the eastern Arabian Sea, Earth Planet. Sci. Lett., 177(3–4), 209–218, doi:10.1016/S0012-821X(00)00053-4, 2000.

Schmidt, H., Czeschel, R. and Visbeck, M.: Seasonal variability of the Arabian Sea intermediate circulation and its impact on 745 seasonal changes of the upper oxygen minimum zone, Ocean Sci., 16(6), 1459–1474, doi:10.5194/os-16-1459-2020, 2020.

Schmiedl, G., de Bovée, F., Buscail, R., Charrière, B., Hemleben, C., Medernach, L. and Picon, P.: Trophic control of benthic foraminiferal abundance and microhabitat in the bathyal Gulf of Lions, western Mediterranean Sea, Mar. Micropaleontol., 40(3), 167–188, doi:https://doi.org/10.1016/S0377-8398(00)00038-4, 2000.

Schmiedl, G., Kuhnt, T., Ehrmann, W., Emeis, K.-C., Hamann, Y., Kotthoff, U., Dulski, P. and Pross, J.: Climatic forcing of 750 eastern Mediterranean deep-water formation and benthic ecosystems during the past 22 000 years, Quat. Sci. Rev., 29(23), 3006–3020, doi:https://doi.org/10.1016/j.quascirev.2010.07.002, 2010.

Schmiedl, G., Milker, Y. and Mackensen, A.: Climate forcing of regional deep-sea biodiversity documented by benthic foraminifera, Earth-Science Rev., 244(May), 104540, doi:10.1016/j.earscirev.2023.104540, 2023.

Schott, F. A. and McCreary, J. P.: The monsoon circulation of the Indian Ocean, Prog. Oceanogr., 51(1), 1–123, doi:10.1016/S0079-6611(01)00083-0, 2001.

Schulte, S., Rostek, F., Bard, E., Rullkötter, J. and Marchal, O.: Variations of oxygen-minimum and primary productivity recorded in sediments of the Arabian Sea, Earth Planet. Sci. Lett., 173(3), 205–221, doi:10.1016/S0012-821X(99)00232-0, 1999.

Schulte, S., Mangelsdorf, K. and Rullkötter, J.: Organic matter preservation on the Pakistan continental margin as revealed by biomarker geochemistry, Org. Geochem., 31(10), 1005–1022, doi:10.1016/S0146-6380(00)00108-X, 2000.

Schulz, H., van Rad, U. and Erlenkeuser, H.: Correlation between Arabian Sea and Greenland climate oscillations of the past 110,000 years, Nature, 393(May), 54–57, doi:10.1038/31750, 1998.

Schulz, M.: On the 1470-year pacing of Dansgaard-Oeschger warm events, Paleoceanography, 17(2), 4–9, doi:https://doi.org/10.1029/2000PA000571, 2002.

Schulz, M. and Mudelsee, M.: REDFIT: Estimating red-noise spectra directly from unevenly spaced paleoclimatic time series, Comput. Geosci., 28(3), 421–426, doi:10.1016/S0098-3004(01)00044-9, 2002.

Schumacher, S., Jorissen, F. J., Dissard, D., Larkin, K. E. and Gooday, A. J.: Live (Rose Bengal stained) and dead benthic foraminifera from the oxygen minimum zone of the Pakistan continental margin (Arabian Sea), Mar. Micropaleontol., 62(1), 45–73, doi:https://doi.org/10.1016/j.marmicro.2006.07.004, 2007.

Sergiou, S., Geraga, M., Rohling, E. J., Rodríguez-Sanz, L., Hadjisolomou, E., Paraschos, F., Sakellariou, D. and Bailey, G.: Influences of sea level changes and the South Asian Monsoon on southern Red Sea oceanography over the last 30 ka, Quat. Res., 110, 114–132, doi:DOI: 10.1017/qua.2022.16, 2022.

Shenoi, S., Shetye, S. R., Gouveia, A. D. and Michael, G. S.: Salinity extrema in the Arabian Sea, Mitt. Geol.-Paläont. Inst. Univ. Hamburg, SCOPE/UNEP Sonderband, 76, 37–49, 1993.

Siddall, M., Rohling, E. J., Almogi-Labin, A., Hemleben, C., Meischner, D., Schmelzer, I. and Smeed, D. A.: Sea-level fluctuations during the last glacial cycle, Nature, 423(6942), 853–858 [online] Available from: http://dx.doi.org/10.1038/nature01690, 2003.

Sigman, D. M. and Fripiat, F.: Nitrogen Isotopes in the Ocean, in Encyclopedia of Ocean Sciences (3rd Edition), edited by J. K. Cochran, H. J. Bokuniewicz, and P. L. B. T.-E. of O. S. (Third E. Yager, pp. 263–278, Academic Press, Oxford., 2019.

Sigman, D. M., Altabet, M. A., McCorkle, D. C., Francois, R. and Fischer, G.: The $\delta15N$ of nitrate in the Southern Ocean: Nitrogen cycling and circulation in the ocean interior, J. Geophys. Res. Ocean., 105(C8), 19599–19614, doi:https://doi.org/10.1029/2000JC000265, 2000.

Singh, A. D., Jung, S. J. A., Darling, K., Ganeshram, R., Ivanochko, T. and Kroon, D.: Productivity collapses in the Arabian Sea during glacial cold phases, Paleoceanography, 26(3), 1–10, doi:10.1029/2009PA001923, 2011.

Sinninghe Damsté, J. S., Kuypers, M. M. M., Schouten, S., Schulte, S. and Rullkötter, J.: The lycopane/C31n-alkane ratio as

a proxy to assess palaeoxicity during sediment deposition, Earth Planet. Sci. Lett., 209(1–2), 215–226, doi:10.1016/S0012-821X(03)00066-9, 2003.

Sirocko, F., Sarnthein, M., Lange, H. and Erlenkeuser, H.: Atmospheric summer circulation and coastal upwelling in the Arabian Sea during the Holocene and the last glaciation, Quat. Res., 36(1), 72–93, doi:10.1016/0033-5894(91)90018-Z, 1991.

790 Sirocko, F., Garbe-Schönberg, Dieter and Devey, C.: Processes controlling trace element geochemistry of Arabian Sea sediments during the last 25,000 years, Glob. Planet. Change, 26(1–3), 217–303, doi:10.1016/S0921-8181(00)00046-1, 2000.

Southon, J., Kashgarian, M., Fontugne, M., Metivier, B. and W-S Yim, W.: Marine Reservoir Corrections for the Indian Ocean and Southeast Asia, Radiocarbon, 44(1), 167–180, doi:DOI: 10.1017/S0033822200064778, 2002.

Staubwasser, M., Sirocko, F., Grootes, P. M. and Segl, M.: Climate change at the 4.2 ka BP termination of the Indus valley
795 civilization and Holocene south Asian monsoon variability, Geophys. Res. Lett., 30(8), 1425, doi:10.1029/2002GL016822, 2003.

Steig, E. J., Jones, T. R., Schauer, A. J., Kahle, E. C., Morris, V. A., Vaughn, B. H., Davidge, L. and White, J. W. C.: Continuous-Flow Analysis of $\delta17O$, $\delta18O$, and δD of H2O on an Ice Core from the South Pole, Front. Earth Sci., 9, doi:10.3389/feart.2021.640292, 2021.

800 Stocker, T. F. and Johnsen, S. J.: A minimum thermodynamic model for the bipolar seesaw, Paleoceanography, 18(4), n/a-n/a, doi:10.1029/2003PA000920, 2003.

Stoffers, P. and Ross, D. A.: Late Pleistocene and Holocene sedimentation in the Persian Gulf—Gulf of Oman, Sediment. Geol., 23(1), 181–208, doi:https://doi.org/10.1016/0037-0738(79)90014-9, 1979.

Stuiver, M. and Braziunas, T. F.: Sun, ocean, climate and atmospheric 14CO2 : an evaluation of causal and spectral
805 relationships, The Holocene, 3(4), 289–305, doi:10.1177/095968369300300401, 1993.

Suthhof, A., Ittekkot, V. and Gaye-Hakke, B.: Millennial-scale oscillation of denitrification intensity in the Arabian Sea during the late Quaternary and its potential influence on atmospheric N20 and global climate, Glob. Biogeochem. Cycles, 15(0), 637–649, 2001.

Szarek, R.: Biodiversity and biogeography of recent benthic foraminiferal assemblages in the south-western South China Sea
810 (Sunda Shelf), University of Kiel., 2001.

Tesdal, J.-E., Galbraith, E. D. and Kienast, M.: Nitrogen isotopes in bulk marine sediment: linking seafloor observations with subseafloor records, Biogeosciences, 10(1), 101–118, doi:10.5194/bg-10-101-2013, 2013.

Thamban, M., Kawahata, H. and Rao, V. P.: Indian summer monsoon variability during the holocene as recorded in sediments of the Arabian Sea: Timing and implications, J. Oceanogr., 63(6), 1009–1020, doi:10.1007/s10872-007-0084-8, 2007.

815 Torrence, C. and Compo, G. P.: A practical guide to wavelet analysis, Bull. Am. Meteorol. Soc., 79(1), 61–78, 1998.

Vogts, A., Moossen, H., Rommerskirchen, F. and Rullkötter, J.: Distribution patterns and stable carbon isotopic composition of alkanes and alkan-1-ols from plant waxes of African rain forest and savanna C3 species, Org. Geochem., 40(10), 1037–1054, doi:10.1016/j.orggeochem.2009.07.011, 2009.

Wakeham, S. G.: Organic biogeochemistry in the oxygen-deficient ocean: A review, Org. Geochem., 149, 104096,

820 doi:https://doi.org/10.1016/j.orggeochem.2020.104096, 2020.

Wakeham, S. G., Freeman, K. H., Pease, T. K. and Hayes, J. M.: A photoautotrophic source for lycopane in marine water columns, Geochim. Cosmochim. Acta, 57(1), 159–165, doi:https://doi.org/10.1016/0016-7037(93)90476-D, 1993.

Wang, L., Sarnthein, M., Erlenkeuser, H., Grimalt, J., Grootes, P., Heilig, S., Ivanova, E., Kienast, M., Pelejero, C. and Pflaumann, U.: East Asian monsoon climate during the Late Pleistocene: high-resolution sediment records from the South

825 China Sea, Mar. Geol., 156(1), 245–284, doi:https://doi.org/10.1016/S0025-3227(98)00182-0, 1999.

Wang, P., Clemens, S., Beaufort, L., Braconnot, P., Ganssen, G., Jian, Z., Kershaw, P. and Sarnthein, M.: Evolution and variability of the Asian monsoon system: State of the art and outstanding issues, Quat. Sci. Rev., 24(5–6), 595–629, doi:10.1016/j.quascirev.2004.10.002, 2005a.

Wang, Y., Cheng, H., Edwards, R. L., He, Y., Kong, X., An, Z., Wu, J., Kelly, M. J., Dykoski, C. A. and Li, X.: The Holocene

830 Asian Monsoon: Links to Solar Changes and North Atlantic Climate, Science (80-.)., 308(5723), 854 LP – 857 [online] Available from: http://science.sciencemag.org/content/308/5723/854.abstract, 2005b.

Wang, Y. J., Cheng, H., Edwards, R. L., An, Z. S., Wu, J. Y., Shen, C.-C. and Dorale, J. A.: A High-Resolution Absolute-Dated Late Pleistocene Monsoon Record from Hulu Cave, China, Science (80-.)., 294(5550), 2345–2348, doi:10.1126/science.1064618, 2001.

835 Wang, Z., DiMarco, S. F., Jochens, A. E. and Ingle, S.: High salinity events in the northern Arabian Sea and Sea of Oman, Deep Sea Res. Part I Oceanogr. Res. Pap., 74, 14–24, doi:https://doi.org/10.1016/j.dsr.2012.12.004, 2013.

Xu, D., Lu, H., Chu, G., Wu, N., Shen, C., Wang, C. and Mao, L.: 500-year climate cycles stacking of recent centennial warming documented in an East Asian pollen record, Sci. Rep., 4(1), 3611, doi:10.1038/srep03611, 2014.

Zhou, Y., Gong, H. and Zhou, F.: Responses of Horizontally Expanding Oceanic Oxygen Minimum Zones to Climate Change

840 Based on Observations, Geophys. Res. Lett., 49(6), e2022GL097724, doi:https://doi.org/10.1029/2022GL097724, 2022.
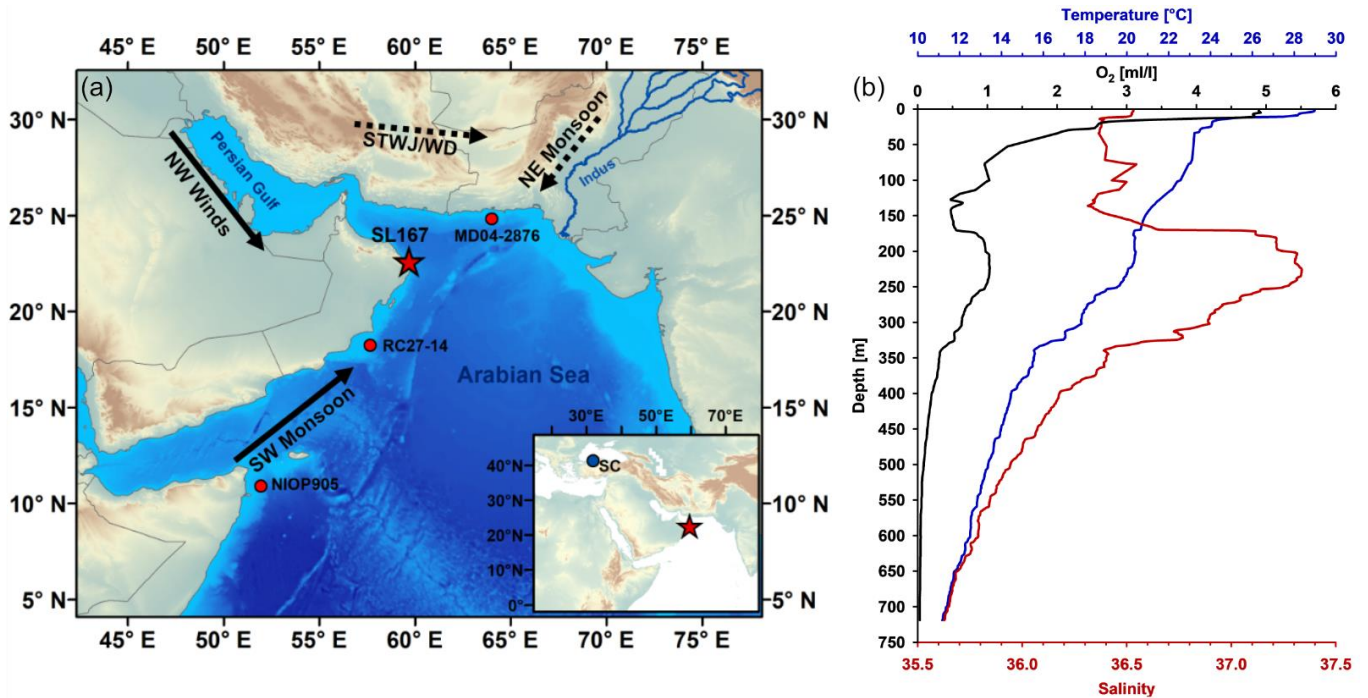
Figure 1: (a) Map of the study site SL167 (red star), nearby marine records (red circles) MD04-2876 (Pichevin et al., 2007), RC27-14 (Altabet et al., 2002), NIOP905 (Ivanochko et al., 2005) and stalagmite record (blue circle in inset map) Sofular Cave (SC)(Fleitmann et al., 2009). The black arrows (SW monsoon & NW winds) show the prevailing wind pattern during the summer and the dashed black arrows (NE monsoon & subtropical westerly jet/western disturbances (STWJ/WD)) indicate the prevailing wind pattern during the winter (after Clift and Plumb, 2008; Hunt et al., 2018). Map was created using ArcGIS v.10.8 (ESRI, 2019). The bathymetric data are from the General Bathymetric Chart of the Oceans (GEBCO, 2014; http://www.gebco.net, last access: 4 January 2017). (b) Temperature (blue), oxygen (O_2, black) and salinity (red) depth profile obtained at the end of the SW-monsoon season in September 2007 during M74/1b cruise at the location of SL167.
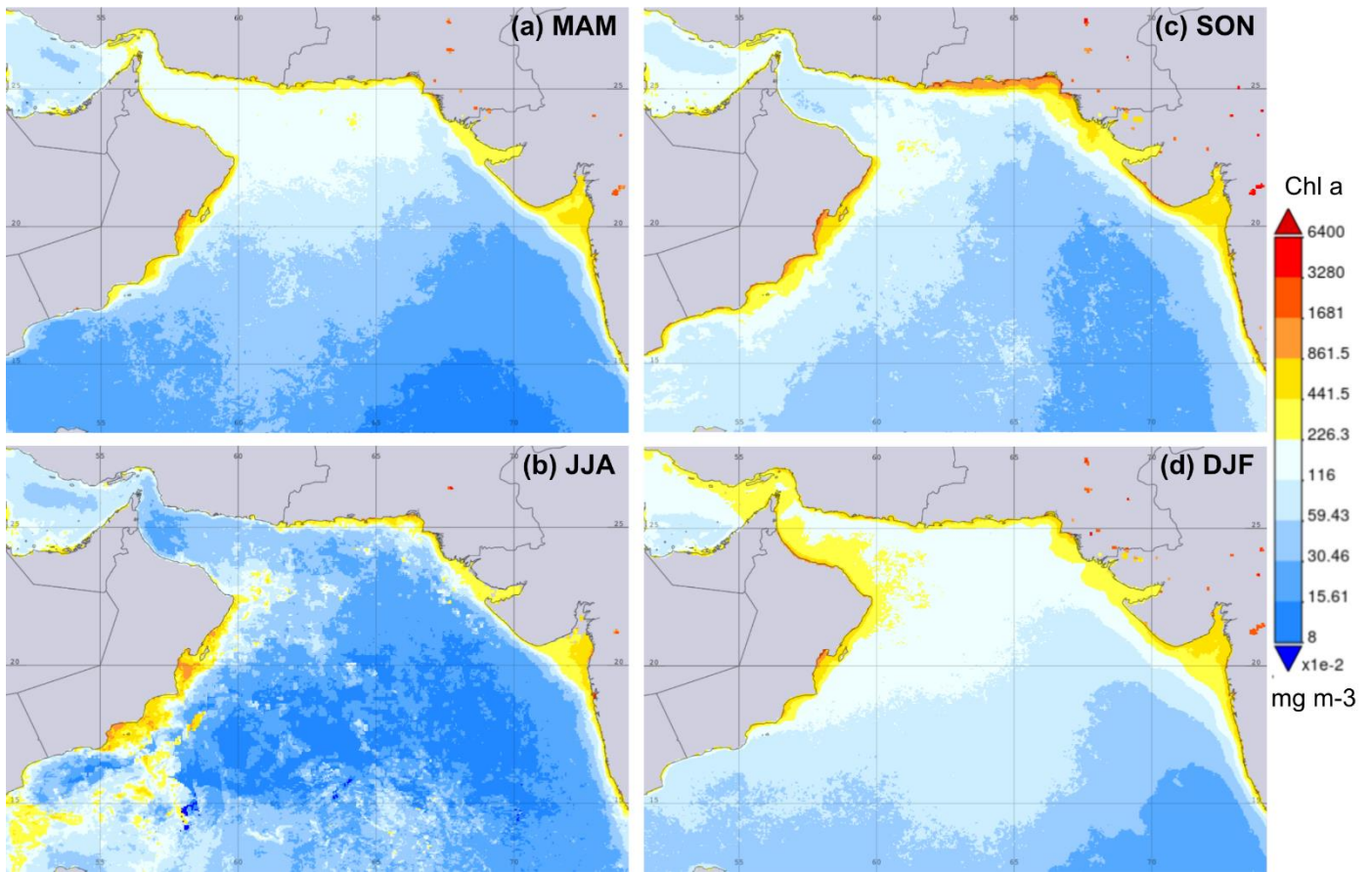
855

Figure 2: Average chlorophyll a concentration (MODIS Aqua, L3m, 4 km spatial resolution, monthly) for the different seasons (a) March, April, May (MAM), (b) June, July, August (JJA), (c) September, October, November (SON) and (d) December, January, February (DFJ) over the period from 2002 to 2022 (NASA, 2022). Data were visualized using the Giovanni online data system, developed and maintained by the NASA GES DISC (date of access: 01/26/2023).

860
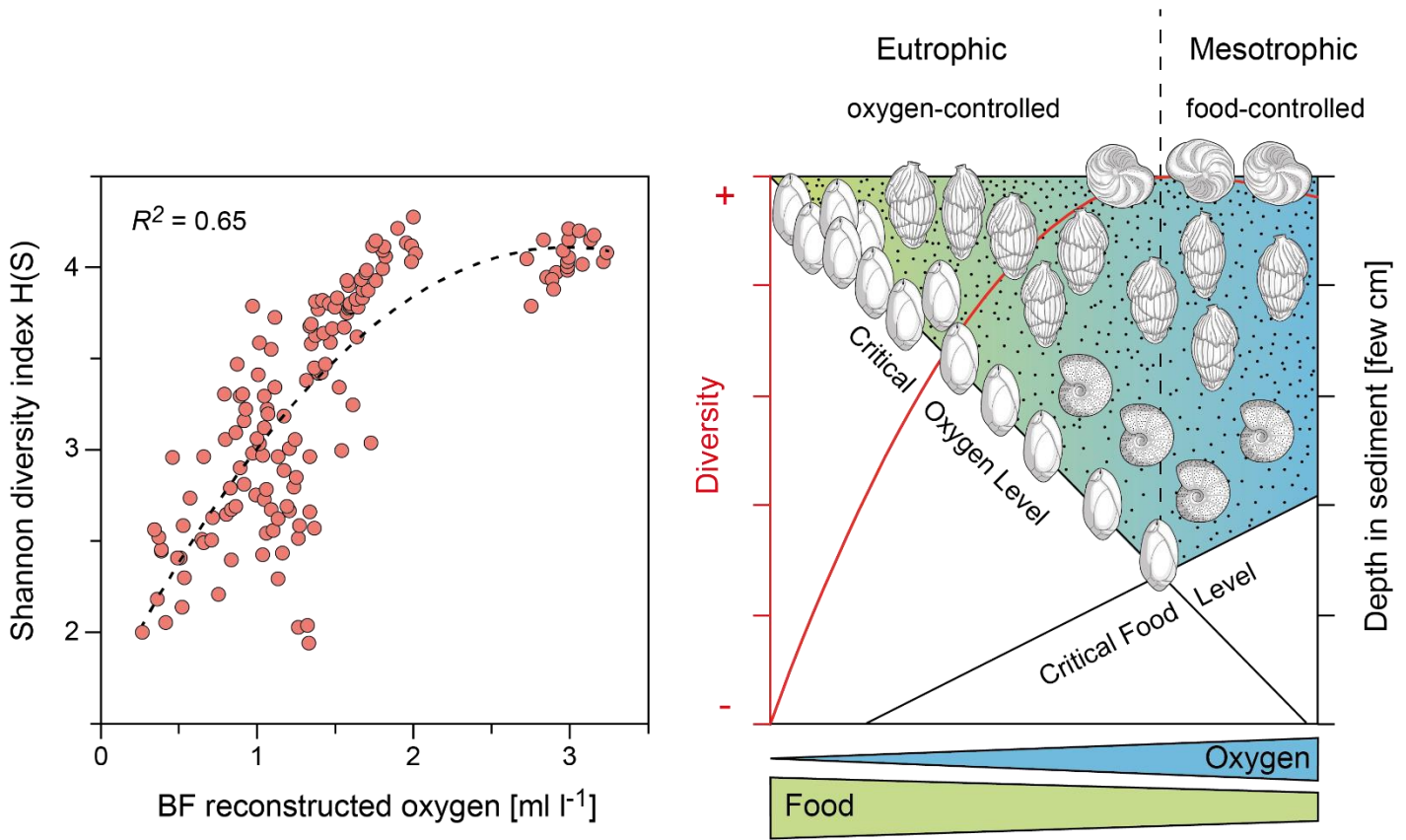
Figure 3: Right: Eutrophic to mesotrophic section of the Trophic-Oxygen (TROX) model of (Jorissen et al., (1995) with addition of (Gooday, (2003) describing the general dependence of benthic foraminiferal microhabitat structure and diversity from oxygen concentration and food supply. Figure modified from (Schmiedl et al., (2023). Left: Reconstructed dissolved oxygen concentration of bottom and pore waters versus benthic foraminiferal diversity H(S) for core SL167. The stippled line represents a polynomial of 2nd degree model with p < 0.001. The observed significant correlation suggests a dominant oxygen control of benthic foraminiferal diversity at site SL167.
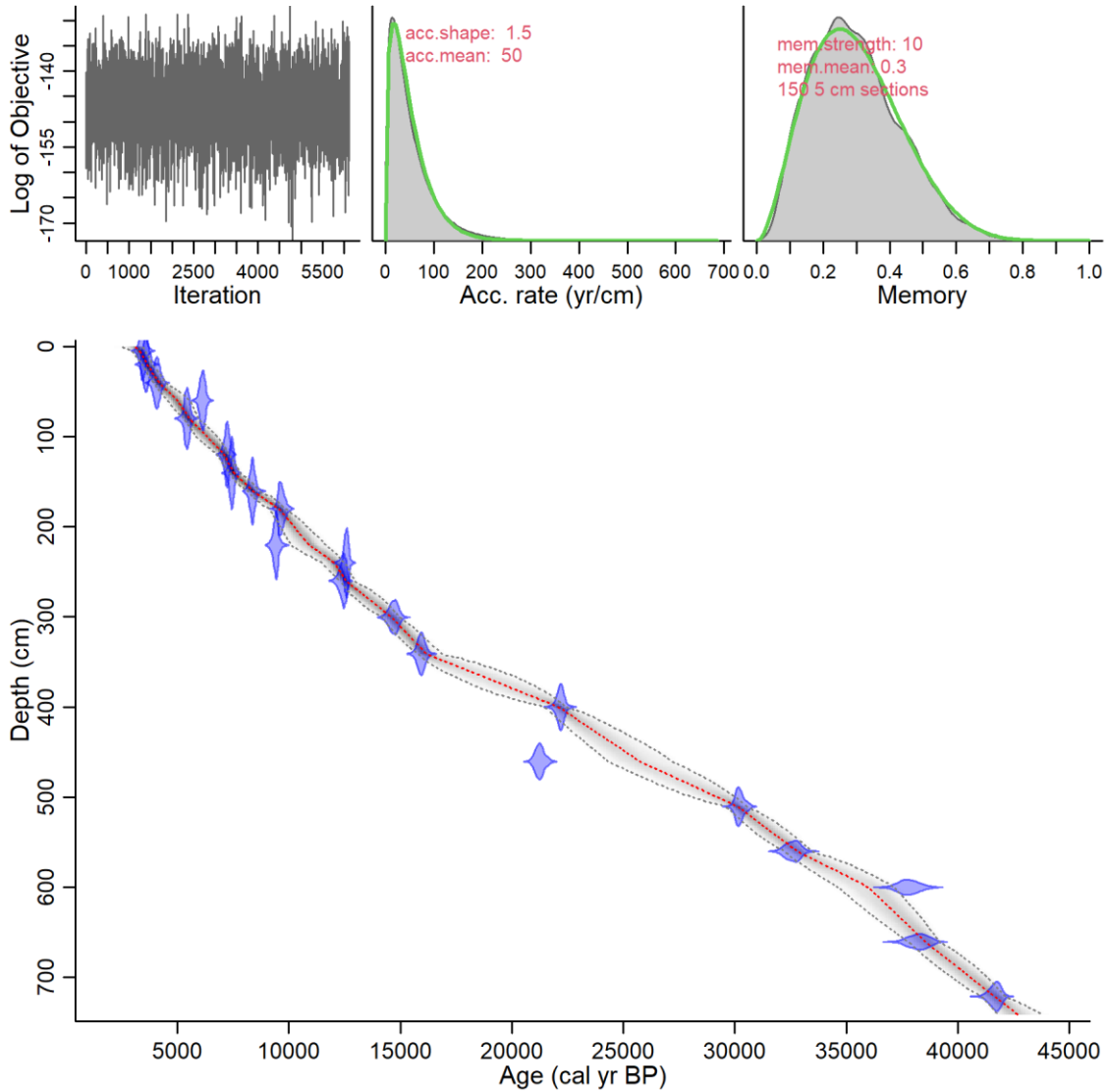
Figures:

Figure 43: **Age-depth model of SL167 using the R package BACON v. 2.5.6 (Blaauw and Christen, 2011). The upper panels show the Markov Chain Monte Carlo iterations (left), the distributions of the prior (green curve) and posterior (grey area) accumulation rates (middle) and memory (right). The lower panel shows the age-depth model of SL167. The calibrated ^{14}C dates are shown in blue. The red line shows the modelled mean age of SL167 with the 95 % confidence interval (black dotted lines). A ΔR of 93 ± 61 years was applied.**
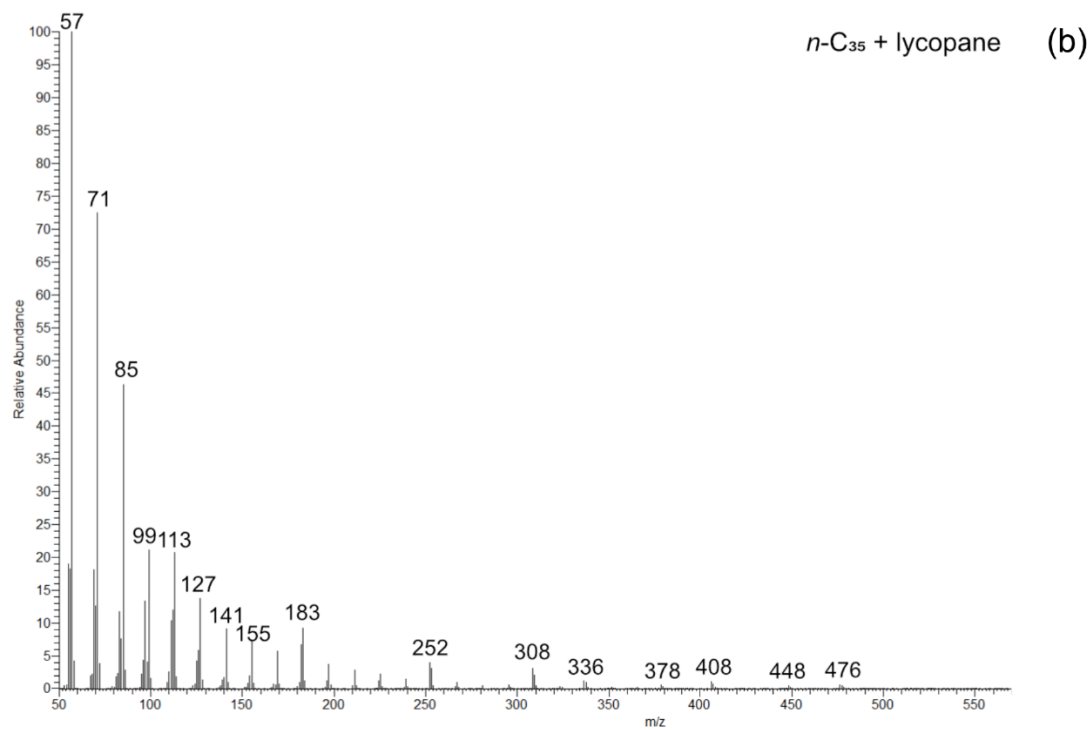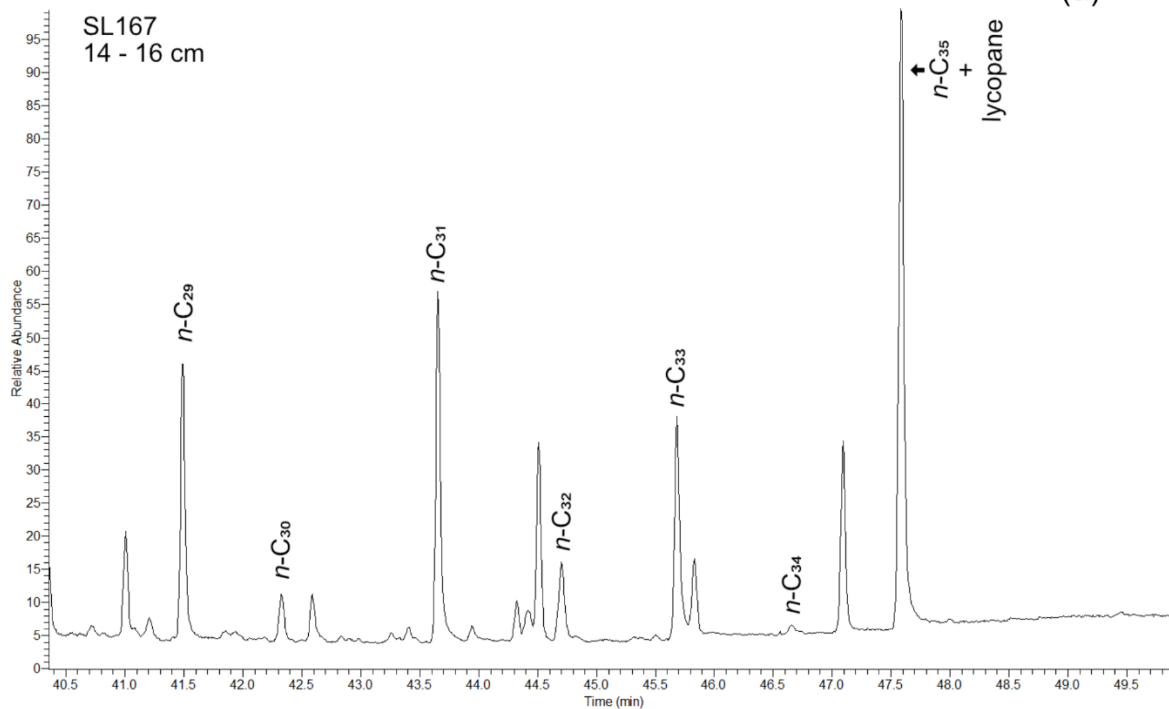
Figure 54: GC-MS measurement of the apolar fraction of sample 14-16 cm with retention time (a) and mass spectra of the *n*-alkane C$_{35}$ + ~~lycopene~~ lycopane (b).
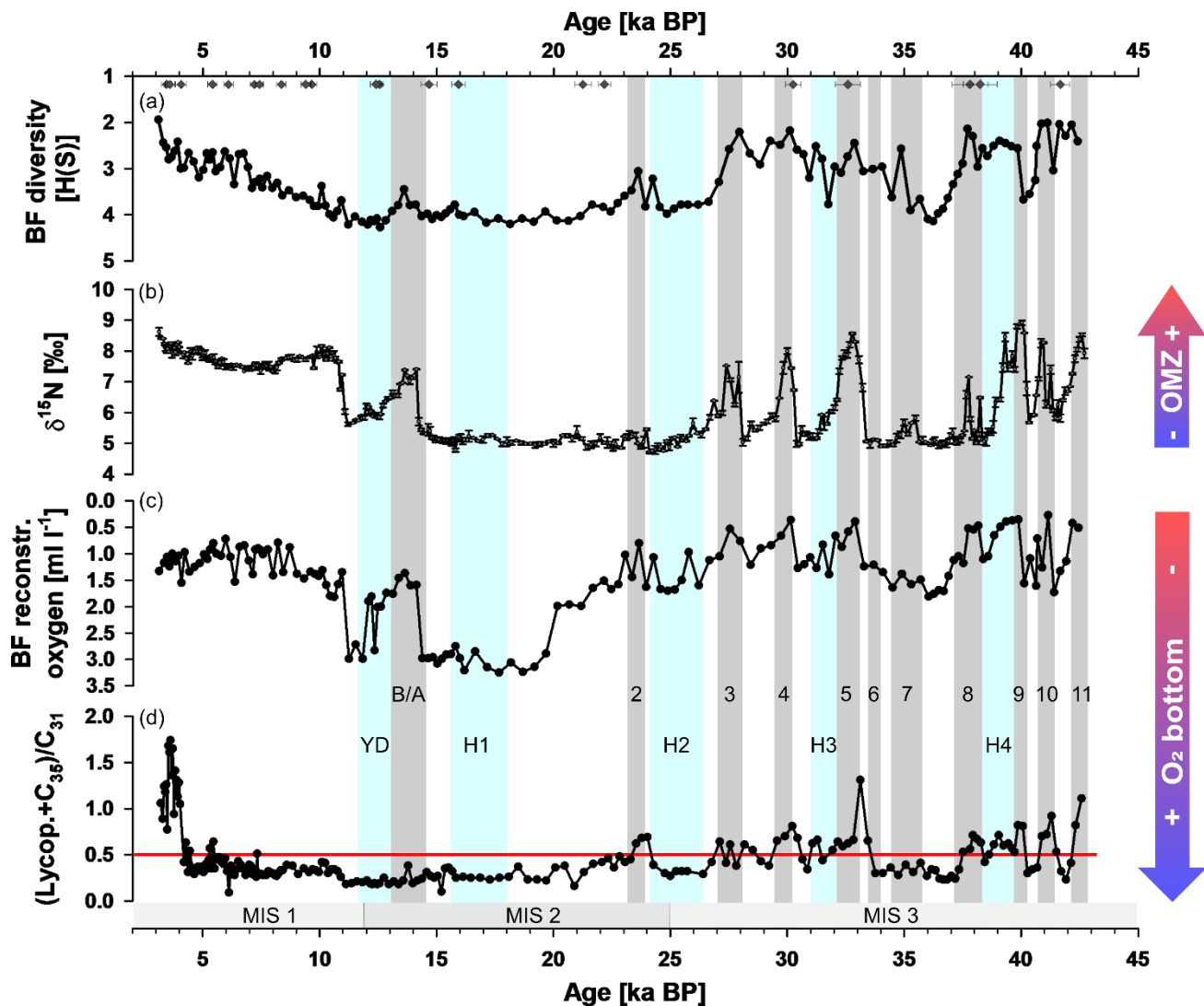
Figure 65: Oxygen proxies of SL167. Shannon Wiener (H(S)) diversity index for benthic foraminifera (BF, a), nitrogen isotope values (δ^{15}N) as denitrification and oxygen minimum zone (OMZ) strength indicator for the water column (b), reconstructed bottom water oxygen content by benthic foraminifera (c) and ratio of (lycopane + n-C$_{35}$)/n-C$_{31}$ as indicator for bottom water oxygen (d). The ~~brown red~~ line in (d) indicates the threshold of oxic to sub-/anoxic conditions (Sinninghe Damsté et al., 2003). Grey bars indicate Bølling/Allerød (B/A) and Dansgaard-Oeschger events (D/O, numbers) mostly based on Fleitmann et al. (2009). Blue bars indicate Younger Dryas based on Fleitmann et al. (2009) and Heinrich (H) events based on a compilation by Allard et al. (2021). Diamonds showing dated ages of SL167. Note the reversed axes for H(S) and BF reconstructed oxygen. The grey bars at the bottom represents the different Marine Isotope Stages (MIS).
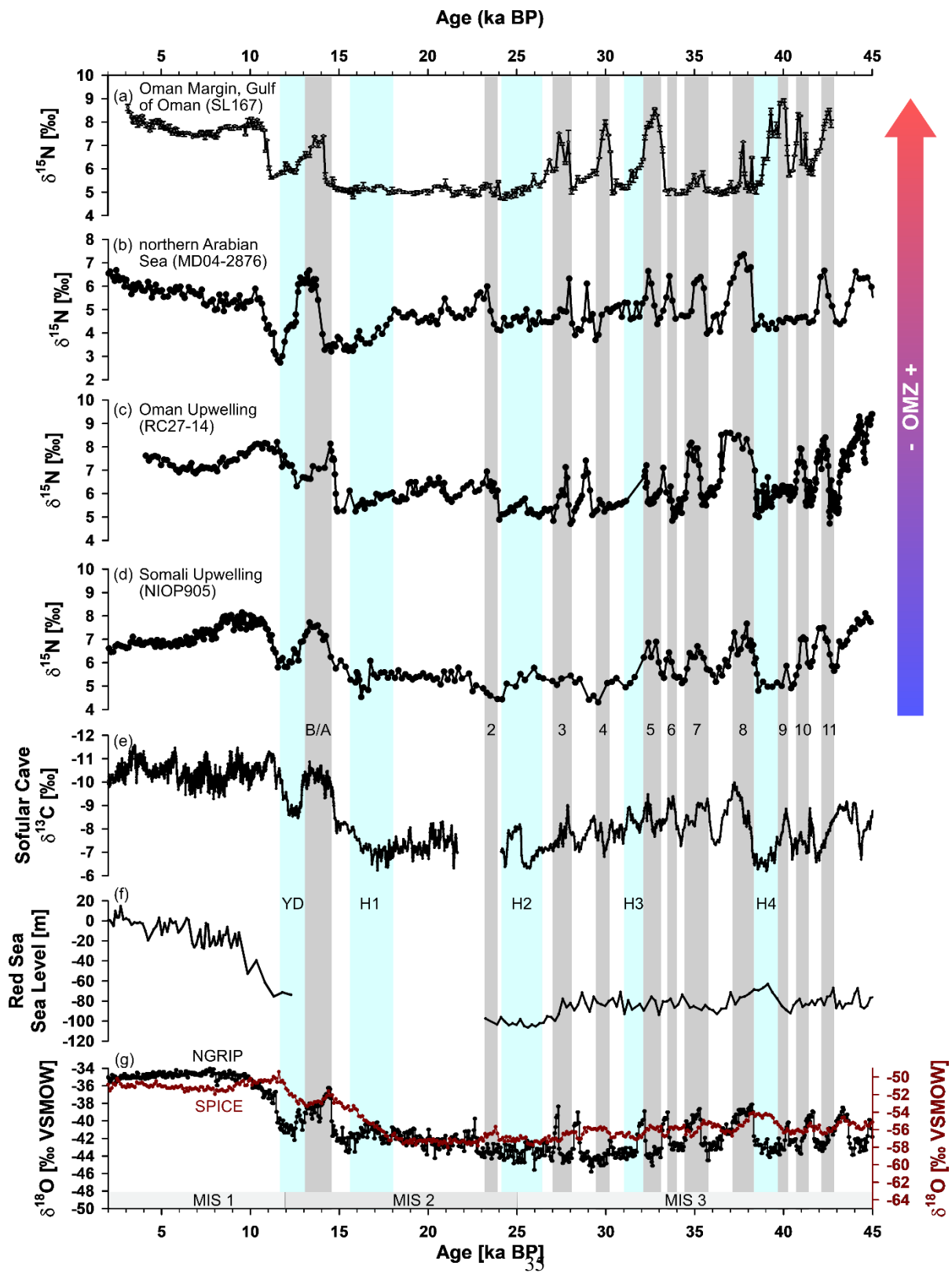
890 **Figure 76: Comparison of high-resolution nitrogen isotope (δ¹⁵N) records in the Arabian Sea. SL167 (this study) from the Gulf of Oman (a), MD04-2876 (Pichevin et al., 2007) from the Pakistan margin in the northern Arabian Sea (b)NIOP905 (Ivanochko et al., 2005) from the Somali Upwelling in the southwestern Arabian Sea (b), RC27-14 (Altabet et al., 2002) from the Oman Upwelling region in the western Arabian Sea (c) and MD04-2876 (Pichevin et al., 2007) from the Pakistan margin in the northern Arabian Sea (d) NIOP905 (Ivanochko et al., 2005) from the Somali Upwelling in the southwestern Arabian Sea (d). Grey bars indicate**
895 **Bølling/Allerød (B/A) and Dansgaard-Oeschger events (D/O, numbers) mostly based on the δ¹³C Sofular cave record (e) by Fleitmann et al. (2009). Combined Red Sea Sea Level reconstruction of sediment core KL11 (f) by Siddall et al. (2003) and Rohling et al. (2008) for the Holocene and Pleistocene parts, respectively. The δ¹⁸O records of NGRIP (North Greenland Ice Core Project members, 2004) and SPICE (Steig et al., 2021) are shown in (g). Blue bars indicate Younger Dryas based on Fleitmann et al. (2009) and Heinrich (H) events based on a compilation by Allard et al. (2021). and tThe grey bars at the bottom represents the different**
900 **Marine Isotope Stages (MIS).**

Figure 87: Spectral analysis (a)) and wavelet power spectrum (b)) of $\delta^{15}N$ of SL167. Red and blue lines in (a) indicate the red noise level and 95 % confidence interval (CI), respectively. Black numbers show significant periodicities on the 95 % CI. The black lines in (b) indicates the 95 % significance level. The colours in b) represent the power of the wavelet power spectrum, with red (blue) showing high (low) power. The grey shaded area represents the cone of influence.
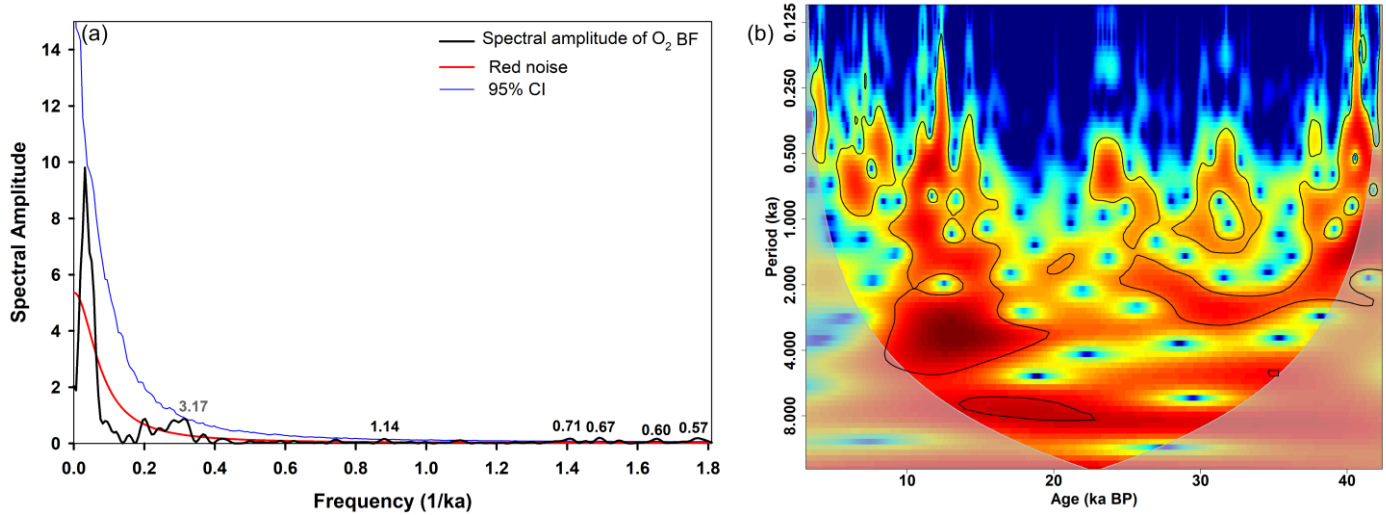
Figure 98: Spectral analysis (a)) and wavelet power spectrum (b)) of the reconstructed oxygen content of SL167 by using benthic foraminifera assemblage (O$_2$ BF). Red and blue lines in (a) indicate the red noise level and 95 % confidence interval (CI), respectively. Black numbers show significant periodicities on the 95 % CI, the grey number (3.17 ka) the significant periodicity on the 90 % CI. The black lines in (b) indicates the 95 % significance level. The colours in b) represent the power of the wavelet power spectrum, with red (blue) showing high (low) power. The grey shaded area represents the cone of influence.

 Tables:

Table 1: AMS ^{14}C dates of planktic foraminifera of sediment core SL167 and calibrated ages using Calib 8.2 with Marine20 calibration curve and ΔR of 93 ± 61 years.

Depth interval (cm)	Mean depth (cm)	Material	^{14}C age (yr BP)	Calendar age 95,4 % prob. (yr BP)	Calendar age max (yr BP)	Calendar age min (yr BP)
4.5–5.5	5	Planktic foraminifera	3790 ± 30	3457 ± 216	3673	3241
19.5–20.5	20	Planktic foraminifera	3910 ± 30	3604 ± 217	3821	3387
40–41	40.5	Planktic foraminifera	4280 ± 30	4083 ± 241	4323	3842
59.5–60.5	60	Planktic foraminifera	6000 ± 30	6112 ± 194	6305	5918
79.5–80.5	80	Planktic foraminifera	5350 ± 30	5425 ± 193	5618	5232
119.5–120.5	120	Planktic foraminifera	7000 ± 30	7216 ± 196	7412	7020
140–141	140.5	Planktic foraminifera	7230 ± 30	7432 ± 171	7602	7261
160–161	160.5	Planktic foraminifera	8160 ± 30	8364 ± 192	8556	8172
179–181	180	Planktic foraminifera	9200 ± 30	9673 ± 225	9897	9448
220–221	220.5	Planktic foraminifera	9010 ± 30	9410 ± 202	9612	9208
239.5–240.5	240	Planktic foraminifera	11300 ± 30	12576 ± 176	12737	12386
259–261	260	Planktic foraminifera	11170 ± 30	12413 ± 241	12654	12172
299–302	300.5	Planktic foraminifera	13080 ± 40	14679 ± 345	15024	14334
340.5–341.5	341	Planktic foraminifera	13980 ± 40	15936 ± 284	16219	15652
399–401	400	Planktic foraminifera	19200 ± 70	22178 ± 263	22441	21915
460–461	460.5	Planktic foraminifera	18430 ± 50	21260 ± 350	21609	20910
510–511	510.5	Planktic foraminifera	26950 ± 120	30252 ± 338	30590	29914
559.5–560.5	560	Planktic foraminifera	29260 ± 140	32593 ± 539	33132	32054
599–601	600	Planktic foraminifera	33930 ± 230	37818 ± 777	38595	37041
660–661	660.5	Planktic foraminifera	34260 ± 220	38255 ± 720	38974	37535
720–722	721	Planktic foraminifera	38290 ± 320	41684 ± 415	42098	41269